Astron. Astrophys. 330, 285–305 (1998)

ASTRONOMY
AND
ASTROPHYSICS

# Quantitative UV spectroscopy of early O stars in the Magellanic Clouds⋆

## The determination of the stellar metallicities

**S.M. Haser**[1], **A.W.A. Pauldrach**[1], **D.J. Lennon**[1], **R.-P. Kudritzki**[1,2], **M. Lennon**[1,2], **J. Puls**[1], **and S.A. Voels**[3]

[1] Universitäts-Sternwarte München, Scheinerstr. 1, D-81679 München, Germany
[2] Max-Planck-Institut für Astrophysik, Karl-Schwarzschild-Str. 1, D-85748 Garching bei München, Germany
[3] Astrophysics Data Facility, Code 631, Goddard Space Flight Center, Greenbelt, Maryland 20771, USA

Received 5 June 1997 / Accepted 29 September 1997

**Abstract.** UV spectra of 4 O-stars in the Magellanic Clouds obtained with the Faint Object Spectrograph of the Hubble Space Telescope are analyzed with respect to metallicity. With the stellar parameters $T_{\rm eff}$, $\log g$, $R_*$, and the mass loss rates $\dot{M}$ known from optical analyses, the metal abundances including iron group elements are derived in two steps. First, hydrodynamic radiation driven wind NLTE models with metallicity as a free parameter are constructed to fit the observed wind momentum rate and thus, yield a dynamical metallicity. Then, synthetic spectra are computed for different metal abundances and compared to the observed spectra to obtain a spectroscopic metallicity. In general, the results obtained from both methods agree.

For the two stars in the Small Magellanic Cloud (NGC 346#3, O3 III(f*) and AV 243, O6 V) metallicities of $\log z/z_\odot = -0.7$ and $-0.8$, respectively, are found. The O3 star shows evidence for CNO-cycled matter in its atmosphere. The metallicity of the two stars in the Large Cloud (Sk$-68^\circ$137, O3 III(f*) and Sk$-67^\circ$166, O4 If$^+$) are constrained to $\log z/z_\odot = -0.3$ and $-0.1$. Because of saturation effects in the cores of the pseudophotospheric metal lines the determination of the LMC metallicity is less reliable.

**Key words:** stars: early type; mass loss – line: profiles – stars: abundances – Magellanic Clouds

### 1. Introduction

Massive stars of spectral type O and B with initial masses ranging roughly from $20 M_\odot$ up to perhaps 200 $M_\odot$ (Kudritzki et al. 1996, Kudritzki 1996) play a key role in the evolution of their host galaxies. Due to their short lifetimes and the final explosion as supernovae of type II, they constitute the most effective recycling factory of galactic matter. During the course of stellar evolution, the mass redelivery to the interstellar medium is substantial due to their strong mass loss in the form of very fast stellar winds, with velocities frequently larger than 2000 km s$^{-1}$, and mass loss rates up to $10^{-5}\, M_\odot\,{\rm yr}^{-1}$. These winds have been shown to be radiation driven by momentum transfer from the stellar photon field to the atmospheric matter via absorption and reemission in the numerous lines of ionized metals, in particular those of the iron group elements (Castor et al. 1975, Pauldrach et al. 1994b and references therein). However since the physical properties and evolution of massive stars are strongly governed by their metallicity (Maeder 1991, 1991b, Leitherer at al. 1992, Maeder & Conti 1994, Langer et al. 1994, Maeder 1996), it is clear that a proper understanding of galactic chemical evolution requires a reliable picture of the physics of massive stars as a function of metallicity.

Given the close inter-relationships between galactic and stellar evolution and metallicity, it is of particular interest to know if precise values for the element abundances of individual O-stars can be obtained from their spectra. As has been shown by the work of Kudritzki et al. (1987) and Pauldrach et al. (1994a, 1994b) this information can best be extracted from the spectroscopic analysis of the ultraviolet spectrum from 1800 Å down to 1150 Å and, preferably, also to the Lyman edge at 911 Å. This spectral region shows fingerprints not only of the lighter elements like C, N, and O in the form of strong P-Cygni profiles, but also blends of hundreds of lines due to iron group ions like Fe IV, Fe V, Fe VI, Ni IV, and Ni V.

The Magellanic Clouds, as the closest companions of our Galaxy, offer an ideal laboratory for this kind of study as has been shown by Walborn et al. (1995a, and references therein). They have presented a spectral atlas of 18 OB stars, 9 in each Cloud, both in the UV and the visible (see Sect. 2 below). They

*Send offprint requests to*: R.P. Kudritzki

⋆ Based on observations with the NASA/ESA *Hubble Space Telescope*, obtained at the Space Telescope Science Institute, which is operated by the Association for Research in Astronomy, Inc., under NASA contract NAS 5-26555.

have pointed out that, from pure "eyeball inspection" and comparison with IUE data for galactic O-stars, there are clear morphological differences in the spectra of the metal poor O-stars in the SMC in comparison to the more metal rich stars in the Galaxy and the Large Magellanic Cloud.

In this paper we attempt to model the UV spectra of four of the O-stars discussed by Walborn et al. We selected a sample of the most massive and hottest stars comprising NGC 346#3 (O3 III(f*) in the SMC plus Sk−68°137 (O3 III(f*) and Sk−67°166 (O4 If+) in the LMC. The star Sk−67°211 (O4 If+) was not considered here since a preliminary analysis of this object was presented by Kudritzki et al. (1996) and also since there were problems related to the determination of a reliable upper bound to the effective temperature due to the absence of He I lines in its spectrum. Sk−67°167 (O4 Inf+) was also excluded since its spectrum is remarkably similar to that of Sk−67°166 and it was thought that this would not contribute much new additional information. As it turned out, deriving metallicities from such hot stars proved difficult and for this reason we added AV 243 (O6 V) to the sample to see if the situation improved for later spectral types.

We examine the wind properties and derive the metallicities by means of spectrum synthesis of the *complete UV spectrum* as it is accessible to the Hubble Space Telescope (Sects. 4 and 5), while particular emphasis will be given to the iron group elements. We will, however, also attempt to derive C, N, and O abundances to decide whether or not CNO cycled matter is present in the photospheres of the individual stars. In Sect. 6 we will summarize and discuss our results.

## 2. The observational data

The ultraviolet spectra were obtained with the *Hubble Space Telescope (HST)* and the *Faint Object Spectrograph (FOS* before *Costar)* under the program IDs 2233/4110 (P.I. R.-P. Kudritzki). The G130H and G190H gratings were used in combination with the 0.25"×2" slit aperture. The spectrograms then covered the wavelength regions 1140 – 1606 Å and 1573 – 2230 Å. The instrumental profile for this aperture is well approximated by a gaussian with a full width at half maximum of 1 Å (G130H), or 1.3 Å (G190H, see the FOS instrument handbook, version 2, p. 11). A formal signal-to-noise ratio (S/N), calculated on the basis of photon statistics, of up to 100 per pixel was achieved, although this also depends on wavelength, for further details see Walborn et al. (1995a).

## 3. Description of the method

The spectra are analyzed using the radiation driven wind model atmosphere code developed in a series of papers (Pauldrach et al. 1986, Pauldrach 1987, Puls 1987, Pauldrach et al. 1994a, 1994b, Taresch et al. 1997 and references therein, Pauldrach et al. 1996) For the sake of brevity we refer the reader to these papers.

The metal abundances are determined in two independent steps. First we calculate consistent hydrodynamical wind models as function of metallicity to fit the observed values of the wind momentum rate $\dot{M}v_\infty$ ($\dot{M}$ is the mass-loss rate and $v_\infty$ is the terminal velocity of the stellar wind). This yields the *dynamical metallicity* $z_{\rm dyn}$.

Then we use a hydrodynamic model atmosphere structure reproducing the observed values of $\dot{M}$ and $v_\infty$ for NLTE spectrum synthesis calculations with varying metallicities to determine the *spectroscopic metallicity* $z_{\rm spec}$.

An important point to note is that our metallicities are at present defined relative to solar ($z_\odot$) by number fraction, the helium to hydrogen ratio being kept fixed at the value derived from the optical analysis. Therefore, when we scale metallicities to obtain $z_{\rm dyn}$ it is clear that the abundance $ratios$, such as [N/Fe] remain fixed at their solar values. Strictly speaking this is incorrect for the Magellanic Clouds, for example it is well established that the carbon and nitrogen abundances in the SMC are significantly depleted relative to iron (Garnett et al 1996). Also, one should bear in mind that when individual element abundances are derived (via the derivation of $z_{\rm spec}$), these are relative to solar. However, there is considerable discussion at present concerning the applicability of solar abundances to early-type Galactic stars given the discrepancies found from detailed analyses of main sequence B-type stars (Gies & Lambert 1992, Kilian 1992, 1994) and how these affect the interpretation of interstellar medium abundances (see the review of Savage & Sembach 1996). For the present we merely emphasize our adoption of the solar abundance ratios. This restriction, however, with its possible implications for the wind dynamics, will be relaxed in future work.

### 3.1. Dynamical metallicities

For the construction of the hydrodynamical models we use the stellar parameters, mass loss rates and terminal velocities as given in Table 1, which have been determined by Puls et al. 1996 (for the determination of $v_\infty$ see also Sect. 3.2).

With these parameters known, the dynamics of radiation driven wind models depend on metallicity only and can, in principle, be used to determine the metallicity. There are two dynamical quantities which can be measured and then compared with the calculations, $\dot{M}$ and $\rm v_\infty$. For given $T_{\rm eff}$ and $R_*$ both parameters depend very strongly on $\log g$ and are very sensitive to errors in the determination of the gravity. However, the product $\dot{M}v_\infty$, or the wind momentum rate, depends only very weakly on the gravity and should be rather insensitive to errors in the gravity, as has been explained by Puls et al. (1996). The observed wind momentum is therefore ideal for a first guess of the metallicity using radiation driven wind models. Having determined $z_{\rm dyn}$ in this way, we investigate at which gravity the individual quantities $\dot{M}$ and $v_\infty$ are reproduced. We then compare these gravities with the corresponding values obtained from the analysis of the optical spectrum.

This method, while theoretically well justified, has one major uncertainty; it relies on the assumption that the hydrodynamics of the radiation driven wind theory as applied in the code are free of serious defects or systematic errors. However

both Lamers and Leitherer (1993) and Puls et al. (1996) have shown that there is a systematic discrepancy between theoretical and observed wind momentum rates as function of "wind performance number" $\eta = \dot{M} v_\infty c / L_*$ ($L_*$ is the stellar luminosity). For high $\eta$ the momentum rate predicted by the theory is too small and it is too high at small $\eta$. Fortunately, all the objects investigated here, except AV243, have $\eta$-values in a range where this discrepancy is small (see Table 1 and Puls et al., 1996). (AV 243 has a very small mass-loss rate for which only an upper limit was determined from $H_\alpha$. This will be discussed further below.) We regard $z_{\rm dyn}$ as an acceptable first guess of the metallicity, but of course this result will be checked by further spectrum synthesis calculations.

### *3.2. Spectrum synthesis*

For the computation of synthetic spectra we adopt the density stratifications and velocity fields of hydrodynamic atmospheric models which reproduce the observed values of $\dot{M}$ and $v_\infty$. Such models were constructed for every star by fitting $z_{\rm dyn}$. Now we use the "line force multiplier parameters" (see Pauldrach et al. 1994 for the definition of these quantities) of these models to recalculate the entire atmospheric structure from deep photospheric layers out to the supersonic wind. Then we adopt ad hoc abundances for all the elements from H to Zn to calculate continuum and line opacities in NLTE and the emergent UV spectrum (for all details see Pauldrach et al., 1994 and Taresch et al., 1997). The abundances are then varied to fit the observed line features in the HST spectra.

For the calculation of synthetic spectra the radiative transfer equation is solved in the observer's frame using the NLTE occupation numbers and the velocity field from the hydrodynamical calculations. This is accomplished with the method of Puls & Pauldrach (1990). The code also accounts for a radially dependent "microturbulence" of the form:

$$v_{\rm turb}(r) = \max \left[ v_{\rm turb}^{\rm min} + v_{\rm turb}^{\rm max} \frac{v(r)}{v_\infty} \right] \quad ,$$

An empirical analysis of P-Cygni profiles of a large sample of galactic and Magellanic Clouds O-stars using IUE and HST spectra has shown that this form of parameterizing the "microturbulence" reproduces the profiles better than a constant value for $v_{\rm turb}$ (Haser et al. 1994b, Haser 1995, Puls et al. 1993). Furthermore it reproduces many morphological aspects present in profiles resulting from multiple nonmonotonic velocity fields of time dependent hydrodynamical calculations (e.g. the so called "extended absorption", Lucy 1982, Puls et al. 1993). $v_{\rm turb}^{\rm max}$ is determined from the steepness of the blue absorption edge and the wavelength position of the emission peak of the P-Cygni profiles.

Figs. 1, 2 and 3 show wind profile fits of our targets for the determination of $v_\infty$ and $v_{\rm turb}$ as described by Haser et al. (1994b) and Haser (1995). The corresponding values are given in Table 1.

For the spectrum synthesis of the complete pseudophostospheric metal line spectrum we adopt $v_{\rm turb}^{\rm min} = 15\,{\rm km\,s^{-1}}$ for $v_{\rm turb}^{\rm min}$. This number is clearly below the sound speed at the relevant temperatures $v_{\rm sound} = \sqrt{\gamma\, kT_{\rm eff}/(\mu m_{\rm H})} \approx 25\,{\rm km\,s^{-1}}$ ($\gamma = 5/3, \mu \approx 1.27$). For the spectrum synthesis this value can be regarded as a technical compromise, since then a wavelength spacing of $\delta\lambda = 0.025$ Å (corresponding to roughly $5\,{\rm km\,s^{-1}}$) is then sufficient to represent the weakest lines with at least 3 points per line. Test calculations have shown, that the metal line spectra do not differ significantly when $v_{\rm turb}^{\rm min} = 5\,{\rm km\,s^{-1}}$ and $\delta\lambda = 0.01$ Å are used instead of the above value of $15\,{\rm km\,s^{-1}}$. We stress here that the remaining discrepancies in the comparison with the observations (see below) can *not* be attributed to the choice of the inner value of the microturbulence.

Pauldrach et al. 1994b introduced a technique (which is also applied here) of adjusting the radiation temperatures $T_{\rm rad}$ below the H- and HeII-Lyman edges such that the effects of the line blocking on the occupation numbers of certain ions are accounted for in an approximate way. This results in reduced photoionization from lower ionization stages and hence the populations of the lower ionization stages are increased. At the relevant effective temperatures these are: C III, C IV, N III, N IV, Si IV.

We also include the effects of X-rays and EUV radiation emitted by shocks in the stellar wind. The method is the same as described by Pauldrach et al. 1994a. The presence of this additional radiation field in the wind works in the opposite direction to line blocking and affects mostly the high ionization stages such as N V, O V, and O VI.

For the determination of iron group element abundances from the weak pseudophotospheric lines in the UV-spectrum, the effects of line blocking and shock emission are of minor importance, as all test calculations have shown.

## 4. Metallicities from wind dynamics

In this section we present the results of the hydrodynamical calculations for the four targets and discuss the derivation of their dynamical metallicities ($z_{\rm dyn}$).

### *4.1. Sk−68°137, O3 III(f*) (LMC)*

Fig. 4 shows the computed stellar wind momentum rates as a function of metallicity indicating a weak dependence on stellar gravity. This dependence can be eliminated by the additional constraint that not only the wind momentum rate but also the terminal velocity $v_\infty$ has to agree with the observations. Therefore we determine, for each gravity, the metallicity fitting the observed wind momentum rate. Then we compare the calculated $v_\infty$ for this pair of gravity and metallicity with the observed value. In this way a $dynamical\ gravity$ $\log g_{\rm dyn}$ is determined, for which the dynamical metallicity $z_{\rm dyn}$ can then be read off (left-hand panel of Fig. 4). The procedure yields $\log g_{\rm dyn} \approx 4.25$ and $\log z_{rmdyn}/z_\odot \approx -0.2$. The dynamical gravity is slightly higher than the value obtained from fitting the optical Balmer lines but with marginal overlap within the errors.

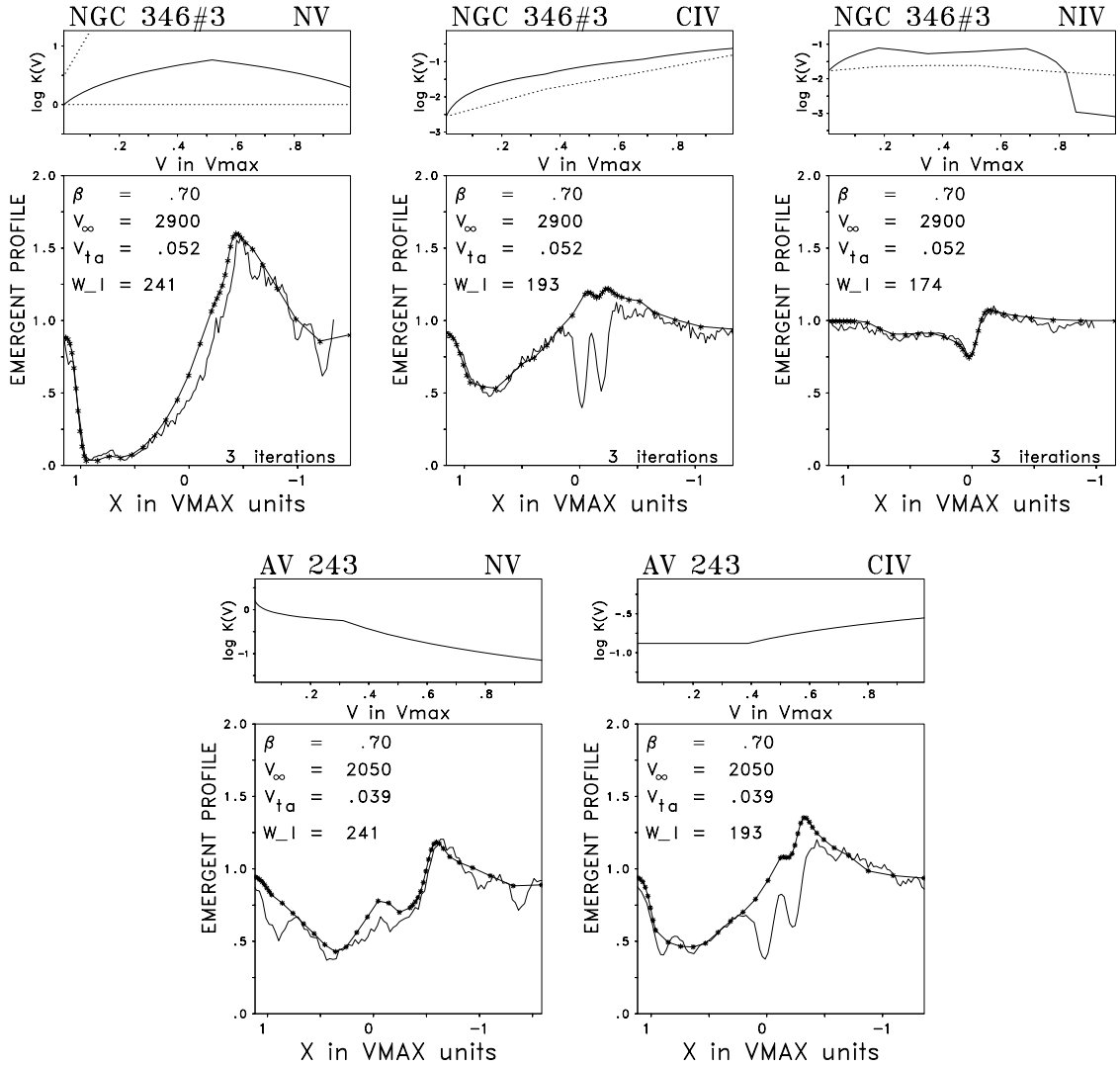


**Fig. 1.** Empirical line fits to the P-Cygni profiles of NGC 346#3 and AV 243. $\beta$ is the exponent which defines the steepness of the velocity law, $v_\infty$ is the derived terminal velocity, $v_{\rm ta}$ is the gaussian turbulence in the outer part of the wind in units of $v_\infty$, $W_{\rm I}$ is the FWHM of the FOS instrumental profile in km s$^{-1}$. The upper panel gives the run of the line strength $k(v)$ which is proportional to the ionization fraction of the considered ion (from Haser 1995, see also Haser et al., 1995).

### *4.2. NGC 346#3, O3 III(f*) (SMC)*

The application of exactly the same procedure as for Sk−68°137 yields $\log g_{\rm dyn} \approx 4.13$ and $\log z_{\rm dyn}/z_\odot \approx -0.8$ for SMC star NGC 346#3, see Fig. 5. Again the dynamical gravity is larger than the spectroscopic value while the metallicity is significantly below solar.

### *4.3. Sk−67°166 O4 If+ (LMC)*

For this object the dependence of wind momentum rate on gravity is much weaker in the relevant range of metallicity yielding $\log z_{\rm dyn}/z_\odot \approx -0.1$ (see Fig. 6, left). The dynamical gravity is $\log g_{\rm dyn} \approx 3.75$ (Fig. 6, right) , again slightly higher than the spectroscopic value.

### *4.4. AV 243, O6 V (SMC)*

This is the coolest star in our sample and the only dwarf. Puls et al. (1996) gave a very high $T_{\rm eff} = 45000$ K for this spectral type. A re-determination using a better spectrogram obtained with the ESO NTT and the EMMI spectrograph has indeed revealed a lower $T_{\rm eff} = 43500^{+2500}_{-1000}$ K, with a gravity $\log g = 3.8^{+0.2}_{-0.1}$ and a He abundance $Y_{\rm He} = 0.1$. Also a larger upper limit for the mass loss rate (Kronberg 1996) was found which now reads $\dot{M} \leq 0.5 \cdot 10^{-6} M_\odot$ yr$^{-1}$.

As for Sk−67°166 the wind momentum rate does not depend on gravity and a dynamical metallicity of $\log z_{\rm dyn}/z_\odot \leq -0.9$ is determined. The dynamical gravity is $\log g_{\rm dyn} \approx 3.72$, again a little smaller than the spectroscopic value.

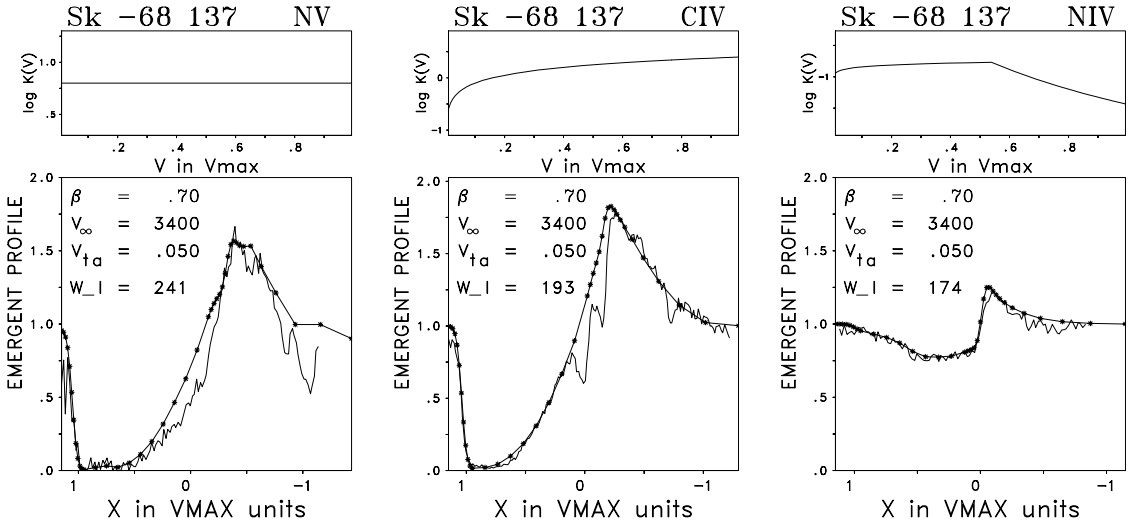


**Fig. 2.** Empirical line fits to the P-Cygni profiles of Sk−68°137, see Fig. 1 (from Haser 1995).

**Table 1.** The stellar parameters $T_{\rm eff}$, $\log g$, $R_*$, mass loss rates $\dot{M}$, and wind efficiencies $\eta$ taken from Puls et al. (1996). $Y_{\rm He} = n_{\rm He}/n_{\rm H}$ is the helium abundance by number relative to hydrogen (the parameters of AV 243 have been redetermined, see text). $v_\infty$ is the terminal velocity and $v_{\rm turb}^{\rm max}$ the gaussian microturbulence in the outer part of the wind. These quantities were derived by the empirical fits to the UV P-Cygni profiles (Haser 1995). Dynamically determined metallicities $z_{\rm dyn}$ and surface gravities $\log g_{\rm dyn}$ as well as the spectroscopic metallicities $z_{\rm spec}$ are also given.

| | **LMC** | | **SMC** | |
|---|---|---|---|---|
| star | Sk−68°137 | Sk−67°166 | NGC 346#3 | AV 243 |
| classif. | O3 III(f*) | O4 If$^+$ | O3 III(f*) | O6 V |
| $T_{\rm eff}$/K | 60000±5000 | 47500±2000 | 55000±5000 | 43500±2000 |
| $\log g$ [cgs] | 4.10±0.15 | $3.65^{+0.15}_{-0.05}$ | $3.90^{+0.15}_{-0.10}$ | 3.80±0.15 |
| $R_*/R_\odot$ | 12.4 | 19.5 | 12.3 | 12.6 |
| $Y_{\rm He}$ | 0.1 | 0.1 | 0.1 | 0.1 |
| $\dot{M}/10^{-6} M_\odot\,{\rm yr}^{-1}$ | $8.0^{+1.5}_{-1.0}$ | $13.0^{+1.0}_{-2.0}$ | $2.3^{+0.4}_{-0.8}$ | $\leq 0.5$ |
| $v_\infty/{\rm km\,s}^{-1}$ | 3400 | 1900 | 2900 | 2050 |
| $v_{\rm turb}^{\rm max}/v_\infty$ | 0.05 | 0.1 | 0.05 | $\leq 0.05$ |
| $\log \dot{M} v_\infty$ [cgs] | 29.23±0.1 | $29.19^{+0.06}_{-0.08}$ | $28.62^{+0.1}_{-0.2}$ | $\leq 27.78$ |
| $\eta$ | 0.73 | 0.70 | 0.26 | $\leq 0.08$ |
| $\log g_{\rm dyn}$ | 4.25 | 3.75 | 4.13 | 3.72 |
| $\log z_{\rm dyn}/z_\odot$ | −0.2 | −0.1 | −0.8 | $\leq -0.9$ |
| $\log z_{\rm spec}/z_\odot$ | −0.3±0.1 | -0.1±0.2 | $-0.7^{+0.2}_{-0.3}$ | $-0.8^{+0.2}_{-0.1}$ |

## 5. Metallicities from spectrum synthesis

As already pointed out above, the computations of the wind dynamics may still be subject to a systematic discrepancy as a function of the performance number $\eta$. We therefore turn to the spectrum synthesis with the following objectives:

1. To examine whether the results, e.g., the metallicities $z_{\rm dyn}$, of the above calculations can be confirmed by a comparison to the UV HST/FOS spectra,
2. To investigate to what extent it is possible to determine individual element abundances, in particular for CNO and Fe.

For the calculation of the synthetic spectra, the atmospheric stratification (density, velocity, temperature) of the best fitting model of Sect. 4 (see Table 1 for the parameters) is taken for each target as a basis for the NLTE calculations of the metal lines with varying abundances.

Before describing the results in detail, two aspects, spectral quality and blending by interstellar lines, need to be discussed.

*Spectral quality.* The accuracy of the analysis depends, of course, on the quality of the spectra. Both the S/N and the wavelength resolution are critical for the work presented here. Given the resolution of the FOS of 1 Å (corresponding to $\approx 200\,{\rm km\,s}^{-1}$, see above) it is clear that only the strongest P-Cygni profiles and interstellar lines can be identified uniquely. All other photospheric features can only be seen as blends since their thermal (or microturbulent) width is about a factor of 10 smaller. On the other hand, we want to point out that a much higher resolution would not help in this respect, because the

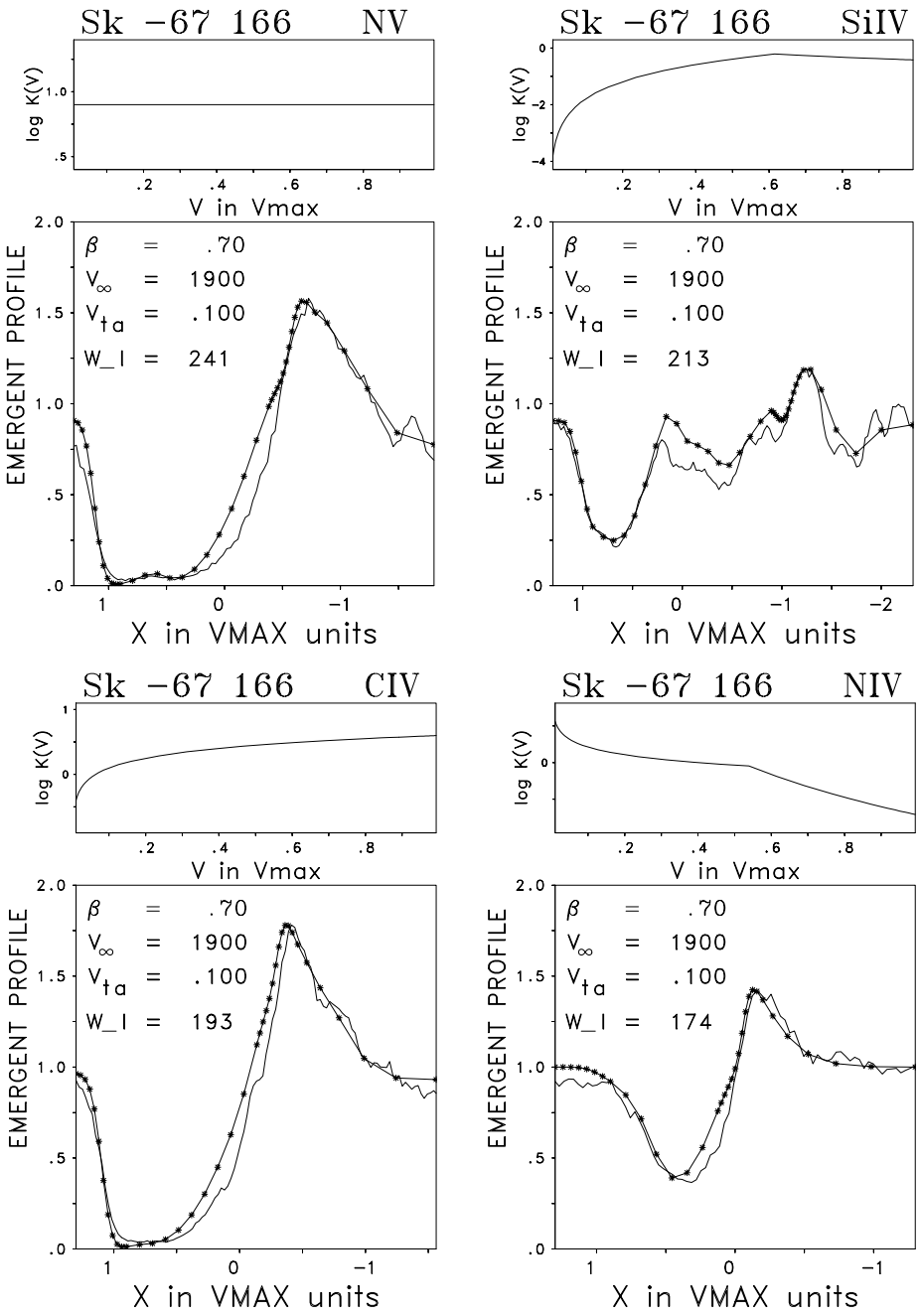


**Fig. 3.** Empirical line fits to the P-Cygni profiles of Sk−67°166, see Fig. 1 (from Haser 1995).

projected equatorial rotational velocity $v_{\rm e} \sin i$ of our targets are about $\approx 100\,{\rm km\,s^{-1}}$ (see Puls et al., 1996). A factor of two better resolution as originally provided by the GHRS in its low resolution mode would have been ideal. With a much higher resolution the distinction between weak stellar blends and weak interstellar lines would have been facilitated (see below), but of course at the expense of much more observing time or less wavelength coverage.

The S/N ratio per resolution element for each star is given in Table 2. These numbers are important to distinguish tiny variations caused by line blends in the synthetic spectra (after convolution to FOS resolution!) from the noise in the observations.

However it is important to consider how the S/N is also limited by instrumental properties, and in the case of FOS the definition of the flat field turns out to be the main source of uncertainty. The data discussed here were flat-fielded following the recommendations in Lindler et al (1993). We used the "superflats" as defined by observations of white dwarfs with the 4.3" aperture. To assume that flat-fielding the data largely removes fixed pattern noise is incorrect, since there are the problems of temporal variations of the flat field plus the question of the applicability of the 4.3" aperture flat field to data obtained with the 0.25"x2.0" slit. As Lindler et al have pointed out, comparison of Science Verification (SV) phase flats and superflats exhibit differences of up to 5–10% , while flat fields derived

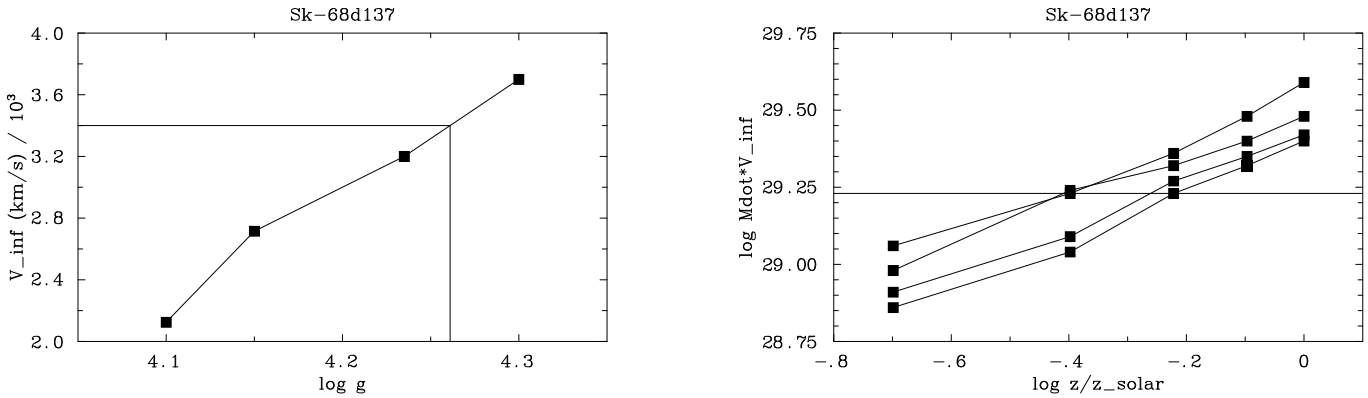


**Fig. 4. left:** Calculated $v_\infty$ as a function of gravity. For each gravity the metallicity yielding the observed wind momentum rate was adopted from the figure on the right. The horizontal line corresponds to the observed value. **right:** Logarithm of wind momentum rate (in cgs) as function of $log(z/z_\odot)$ for different gravities $\log g$ = 4.10, 4.15, 4.23, 4, 30 (from top to bottom). Note that the curves for $\log g$=4.10 and 4.15 do not cross over. The horizontal line corresponds to the observed value.

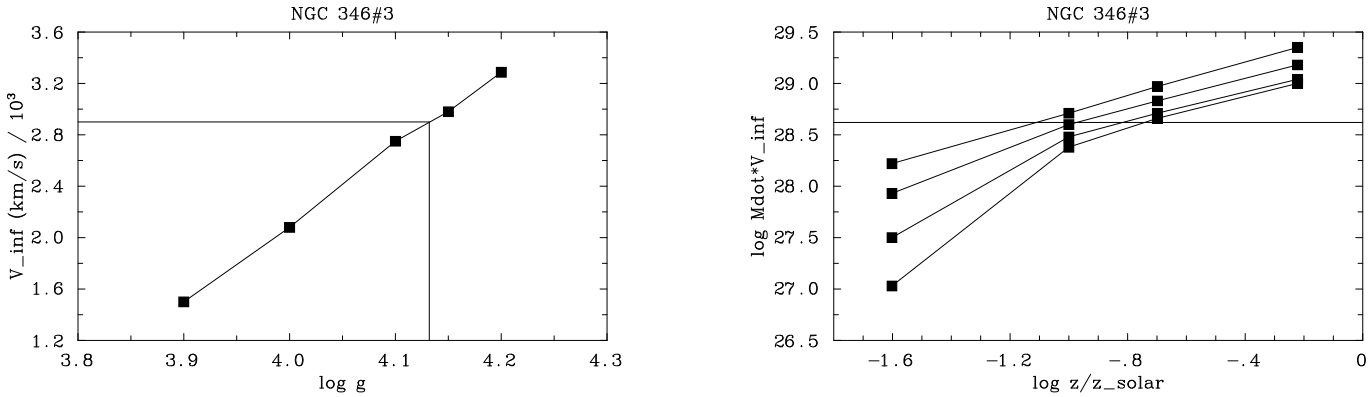


**Fig. 5.** Fit of dynamical metallicity and gravity for NGC 346#3 similar as in Fig. 4. The gravities in the diagram on the right are 3.90, 4.00, 4.10, 4.15 (from top to bottom).

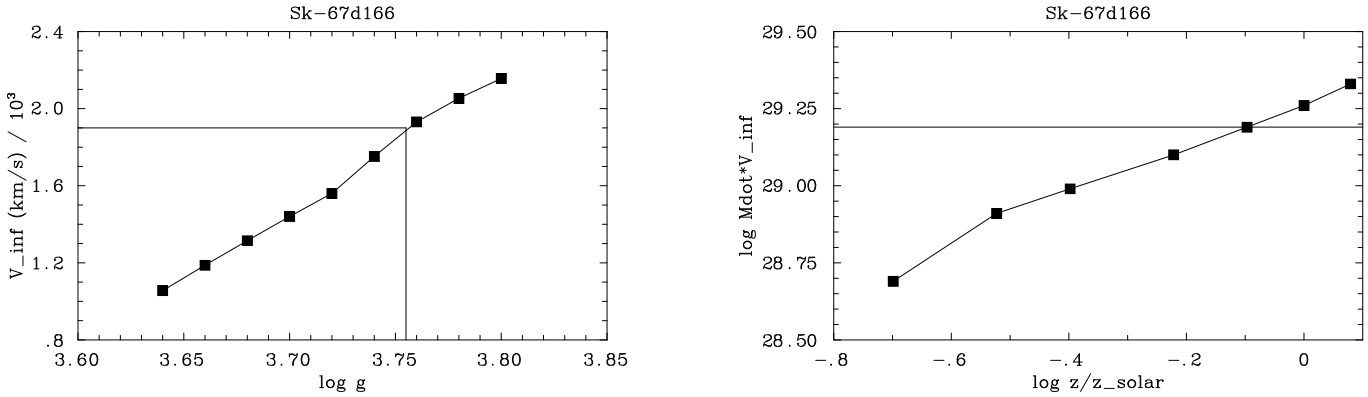


**Fig. 6.** Same as Fig. 4, but for Sk−67°166.

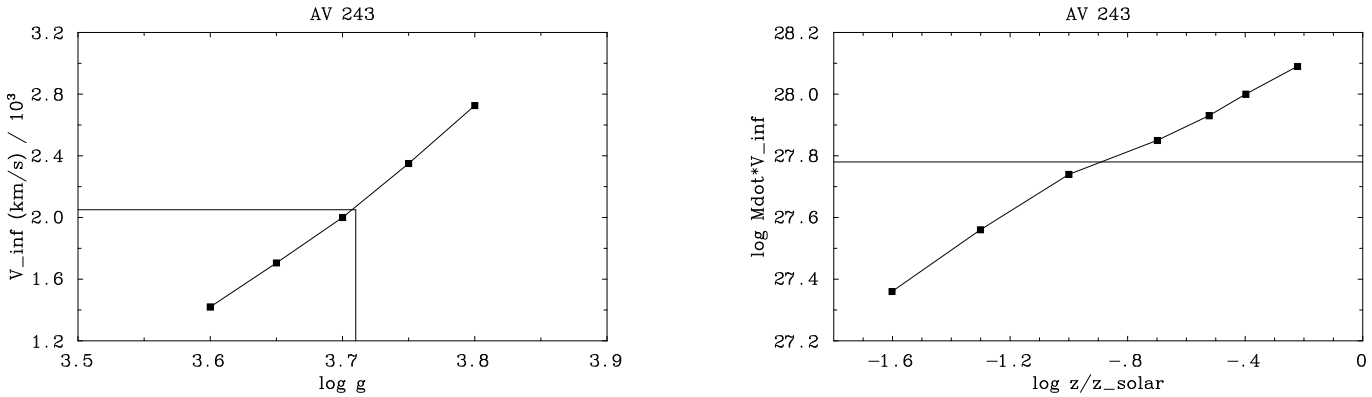


**Fig. 7.** Same as Fig. 4, but for AV 243. Note that the horizontal line in the figure on the right is only an upper limit for the observed wind momentum.

from different apertures also show differences at the 5% level (see also Keyes 1993 and Januzzi & Hartig 1993). They suggest that possible causes of temporal changes could be variations in photocathode/diode response or uncertainties in the y-position of the data resulting from target acquisition errors (which are certainly present). Larger apertures on the other hand will tend to smooth out detector granularity more than the smaller apertures, specific features tend to be narrower and deeper in the flat fields for the smaller apertures. Since we are interested in synthesizing individual features or blends in detail, it is imperative to know what peculiar or anomalous features might be present in the flat field. As we discuss below, we attempt to derive a spectroscopic metallicity using only two small portions of the spectrum and we examined the superflat and the ratio of the SV flat and superflat in these regions. In the first window at 1262 – 1269 Å, fixed pattern noise is only of order 1% in both superflat and superflat/SV flat ratios (there is a mean slope but this is removed in our normalization procedure). In the other window at 1560 – 1594 Å the fixed pattern noise is closer to 2% although there are also two features present at the 4% level in the flat field ratios, and 3 such features in the superflat. However in our comparison of synthetic and observed data we check for correlations between positions of disagreement and these anomalous features. It is clear however that disagreements of order 1 and 2 % in the regions we have just discussed may not be significant, given the uncertainty associated with the flat field.

The spectral analysis is further complicated by the fact that practically nowhere in the spectra below 1600 Å can a unique continuum be defined because of the dense crowding of the lines of the iron group elements. We will discuss this point for each star separately in the following sections.

*Interstellar lines.* Besides those interstellar lines which can be identified immediately (Table 4) there are also numerous weaker lines which cannot be resolved due to the instrumental profile. On the other hand, in the IUE high resolution spectra of two galactic O stars with strong interstellar absorption, these lines are easily detected. As an example, we show the IUE spectrum of the galactic O3-star HD 93129A between 1260 and 1300 Å (Fig. 8, Table 3). Since in the FOS spectra of lower resolution these interstellar lines overlap with the weak stellar lines which shall be used to determine the metal content, the results for $z_{\rm spec}$, the metallicity derived from spectrum synthesis, could be erroneous, if no correction for the presence of interstellar lines is applied.

**Table 2.** S/N per resolution element (1 Å) of the four HST/FOS–spectra at two characteristic wavelengths.

| $\lambda$/ Å | 1300 | 1500 |
|---|---|---|
| NGC 346#3 | 100 | 120 |
| AV 243 | 35 | 45 |
| Sk−67°166 | 40 | 47 |
| Sk−68°137 | 20 | 28 |

### *5.1. NGC 346#3*

The O3-star NGC 346#3 in the SMC has the best FOS spectrum of our targets with regard to S/N. Furthermore, the C IV line is definitely unsaturated, which makes the effects of the line blocking and shock emission easier to recognize and disentangle.

The observed wind momentum rate is best reproduced with $z_{\rm dyn} \approx 0.2$. At this abundance, the synthetic spectrum, too, succeeds in reproducing most of the weak blends of the iron group lines (see Fig. 9). However, before we discuss the spectrum synthesis of the lines of iron group elements in more detail, we want to discuss the abundance fit of the strong P-Cygni profiles of N V$\lambda\lambda$1239, 1242, O V$\lambda$1371, C IV$\lambda\lambda$1548, 1551, and N IV$\lambda$1719. The determination of abundances from these lines is complicated by the fact that the parameters of the shock emission have to be simultaneously determined (see Pauldrach et al 1994b). In addition, the influence of line blocking on the ionizing photospheric radiation field has to be constrained in terms of radiation temperatures between the H- and the He II-Lyman-edge. For a detailed discussion of the method, see Pauldrach et al. (1994b). After running a large number of test models the best fit parameters allowing a simultaneous fit of all the CNO

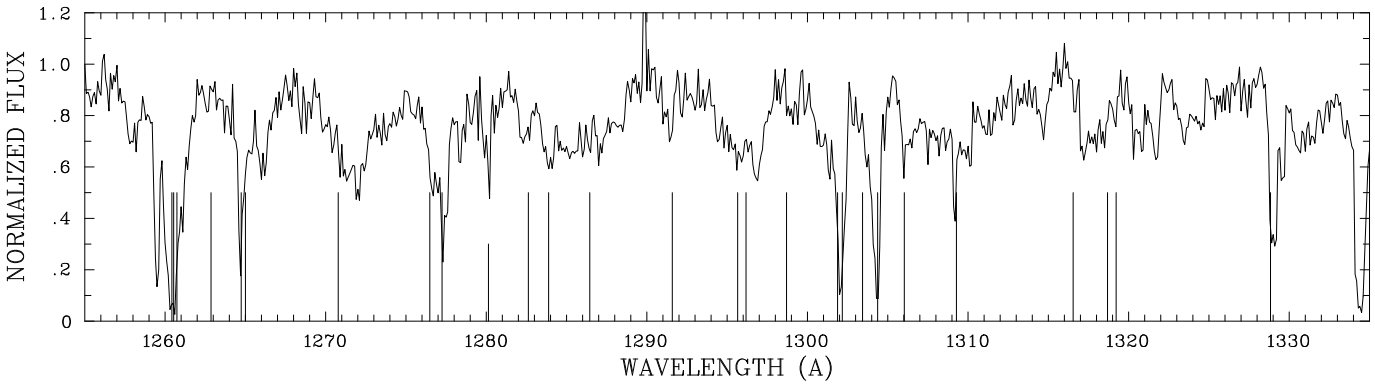


**Fig. 8.** Interstellar lines in the IUE–spectrum of the galactic O3-star HD 93129 A. The vertical lines mark the rest wavelengths of identified and possible interstellar lines, taken from the resonance line list of Morton (1991, s. Table 3). Only lines with an excitation potential $\chi < 300\,\mathrm{cm}^{-1}$ are marked.

**Table 3.** The interstellar lines marked in Fig. 8

| λ (Å) | line | λ (Å) | line |
|---|---|---|---|
| 1262.86 | S I | 1295.65 | S I |
| 1264.74 | Si II | 1296.17 | S I |
| 1265.00 | Si II | 1298.70 | Ti III |
| 1270.78 | S I | 1301.87 | P I |
| 1276.48 | C I | 1306.03 | O I |
| 1277.25 | C I | 1309.28 | Si II |
| 1280.14 | C I | 1316.54 | S I |
| 1282.62 | P I | 1318.68 | P I |
| 1283.88 | P I | 1319.22 | P I |
| 1286.44 | P I | 1328.83 | C I |
| 1291.58 | Ti III | | |

**Table 4.** Strong interstellar lines in the UV between 1150 and 1750 Å. The lines were identified using Morton's (1991) list of resonance lines.

| No. | Linie | λ (Å) | No. | Linie | λ (Å) |
|---|---|---|---|---|---|
| 1 | S III | 1190.21 | 10 | C II | 1334.52 |
| (blend) | Si II | 1190.42 | (blend) | | 1335.71 |
| 2 | Si II | 1193.29 | 11 | Si IV | 1393.76 |
| 3 | N I | 1199.55 | | | 1402.77 |
| (blend) | | 1199.96 | 12 | Si II | 1526.71 |
| | | 1200.22 | 13 | C IV | 1548.20 |
| | | 1200.72 | | | 1550.77 |
| 4 | Si III | 1206.50 | 14 | Fe II | 1608.45 |
| 5 | S II | 1250.58 | 15 | C I | 1656.27 |
| 6 | S II | 1253.81 | (blend) | | 1656.93 |
| 7 | S II | 1259.52 | | | 1657.01 |
| (blend) | Si II | 1260.42 | | | 1657.91 |
| 8 | O I | 1302.17 | | | 1658.12 |
| 9 | O I | 1304.86 | 16 | Al III | 1670.79 |

wind lines mentioned above are given in Table 5. They will be discussed below.

*Nitrogen and Carbon.* The P-Cygni profiles of the carbon and nitrogen ions require an abundance pattern with a strongly depleted carbon abundance $A_\mathrm{C}$ and an enhanced nitrogen abundance $A_\mathrm{N}$. No combination of $T_\mathrm{rad}, L_\mathrm{X}$ and $v_\mathrm{jump}$ succeeds in reproducing both the strength of C IV and N IV while maintaining $A_\mathrm{N} = A_\mathrm{C} = 0.2\,A^\odot$ which was used for all other elements. The maximum of the chosen shock jump velocity ($v_\mathrm{jump} = 220\,\mathrm{km\,s^{-1}}$) distributes the shock emission in a way that both C IVand N IV are weakened substantially (see Pauldrach et al. 1994a). If C IV were to be fitted by the shock emission alone (i.e., without lowering $A_\mathrm{C}$) the N IV line would vanish completely due to enhanced ionization. The given abundances for C and N are thus a compromise between two mechanisms acting in different directions on the ionization balance: the line blocking below the H-Lyman edge and above the HeII-Lyman edge and the shock radiation field. $A_\mathrm{N} = 0.4\,A_\mathrm{N}^\odot$ and $A_\mathrm{C} = 0.02\,A_\mathrm{C}^\odot$ describe the least extreme deviation from $z_\mathrm{spec} = 0.2$ used for all other elements given the possible range for $\log L_\mathrm{X}/L_\mathrm{bol} = -6 \ldots -8$, $v_\mathrm{jump} = 180 \ldots 230\,\mathrm{km\,s^{-1}}$ and various sets for $T_\mathrm{rad}$. They should therefore be regarded as a lower ($A_\mathrm{N}$) and an upper limit ($A_\mathrm{C}$).

The chosen $\log L_\mathrm{X}/L_\mathrm{bol} = -8$ lies at the lower end of the typical range for $L_\mathrm{X}$ for O-stars (see Chlebowski et al., 1989). Nevertheless it is sufficient to saturate the O VI$\lambda\lambda$1032, 1038 line in the outer parts of the wind, as observed with the HUT (Walborn et al., 1995b). (Unfortunately, because of the 3 Å wide instrumental profile no further information about the shock emission can be extracted from the HUT data).

*Oxygen.* The subordinate line of O V poses problems. It always comes out too strong (for the other O3 stars as well, see below), although the abundance has already been reduced to $A_\mathrm{O} = 0.075\,A_\mathrm{O}^\odot$, i.e., by more than a factor of two. Test calculations showed that, in order to reproduce the profile, one would have to reduce the radiation temperature at the exciting resonance line (at 629.73 Å) drastically below 36000 K, the value chosen to reproduce the N IV and C IV profile. However, this would destroy the fit for the latter, an effect that could not be counteracted by the choice of different shock–parameters. Since this problem occurs in all models for all the O3 stars, we do not attempt to fit the line with a lower abundance, which would have

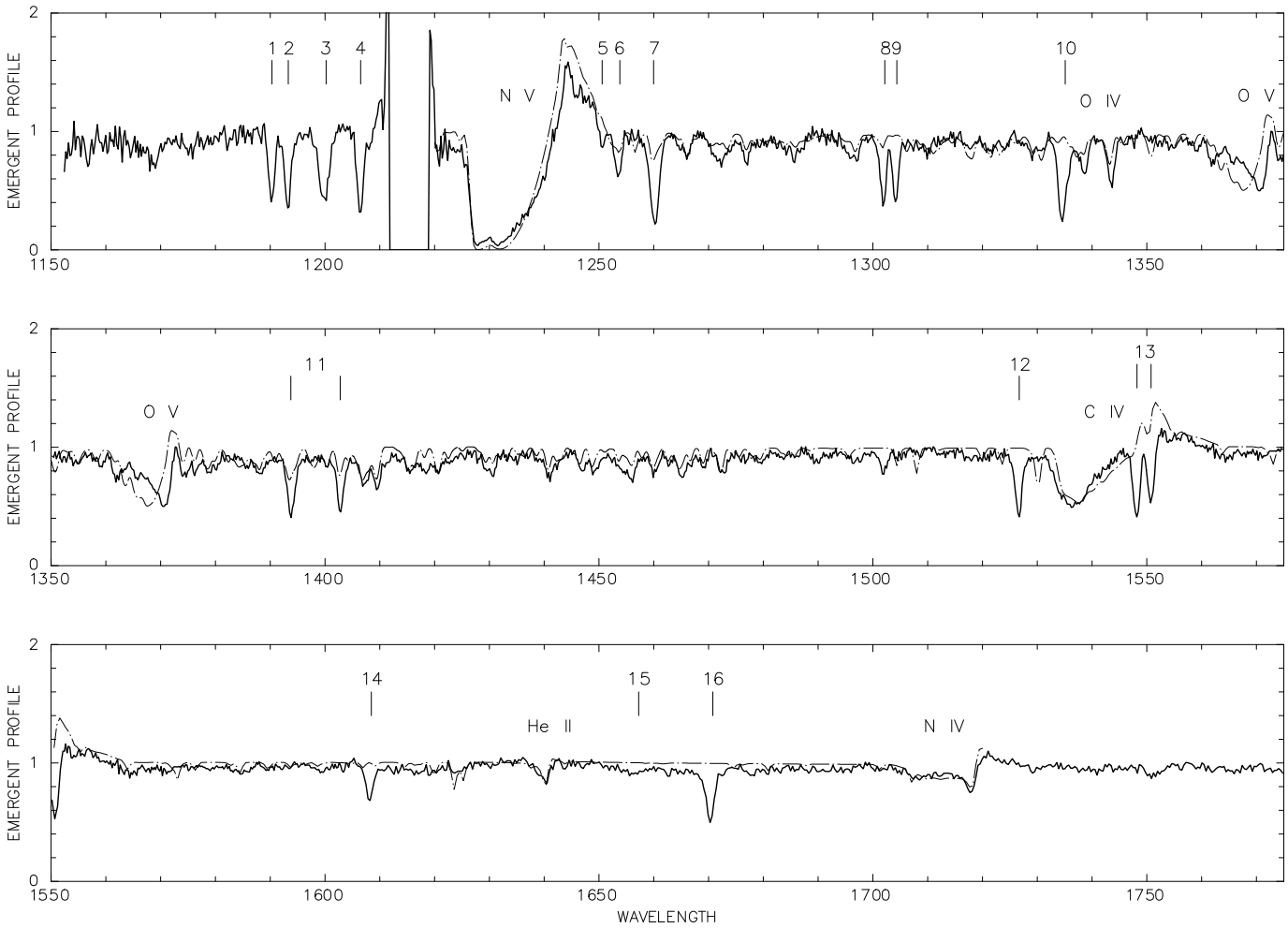


**Fig. 9.** Synthetic spectrum for NGC 346#3 (dash-dotted, $T_{\rm eff}$ = 55000 K, $z_{\rm spec}$ = 0.2, $A_{\rm N}$ = 0.4, $A_{\rm C}$ = 0.02, $A_{\rm O}$ = 0.075) folded with the instrumental profile and compared with the HST–spectrum (heavy). The numbers indicate interstellar absorption lines (see Table 4).

to be drastically smaller than the one for carbon. We regard this as unreasonable from the standpoint of stellar evolution models. We attribute this discrepancy to our approximative treatment of the line blocking. Future models using a selfconsistent blocking algorithm (see Pauldrach et al 1996) will have to be used to discover the reason for this particular discrepancy. The problem is also present in the analysis of the galactic O3 If* star HD 93129 A by Taresch et al. (1997), who used essentially the same procedure.

*Iron and Nickel.* Fortunately, the spectrum synthesis of the much weaker lines of iron and nickel is much less affected by the choice of the parameters in Table 5, since they are formed close to the photosphere, where shock emission is unimportant. Similarly, since the ionization edges of the ionization stages observed and analyzed lie beyond the HeII-edge, blocking is not a dominant factor. The excitation of the levels is not too far from LTE.

In Fig. 9 we compare the synthetic spectrum of the model (convolved with the instrumental profile) using the parameters from Table 5, with the HST spectrum of NGC 346#3. The agreement is generally good "at first glance" (the P-Cygni profiles have already been addressed above). In order to determine the Fe/Ni abundances, however, we have to compare the outcome of a model grid with different $z_{\rm spec}$ to see how sensitively the many blends of the weak iron and nickel lines react. Building upon the hydrodynamic structure for the model with $z_{\rm dyn}$ and $\log g_{\rm dyn}$ as in Table 1, i.e., the same velocity field and the same density structure, we varied the abundances and computed additional synthetic spectra for $z_{\rm spec}$ = 0.1, 0.3, and 0.4 in the regions with strong Fe V, Fe VI, and Ni V lines. These are shown in Fig. 10 *without* convolution with the instrumental profile. It can be seen that, although the mass-loss rate of $\dot{M} = 2.3 \cdot 10^{-6} M_\odot$ yr$^{-1}$ is only moderate and the abundances are rather small, *many*

**Table 5.** Spectrum synthesis parameters for NGC 346#3.

| $\log L_{\rm X}$ | $v_{\rm jump}$ | $T_{\rm rad}$/kK | | |
|---|---|---|---|---|
| [$L_{\rm bol}$] | [km s$^{-1}$] | $< 300$ Å | $< 480$ Å | $< 800$ Å |
| $-8$ | 220 | 46 | 45 | 36 |

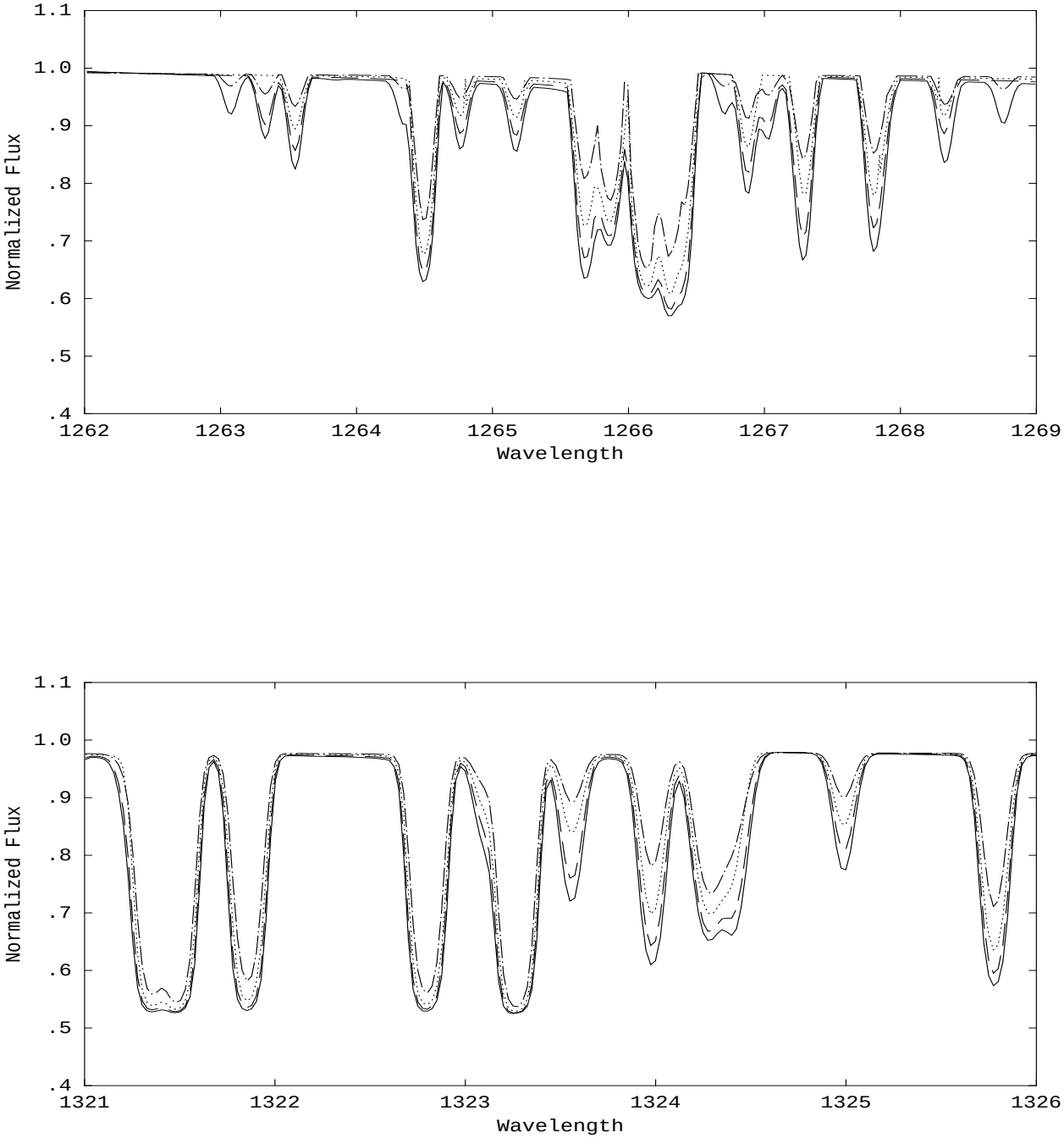


**Fig. 10.** The synthetic spectra of NGC 346#3 for $z = 0.4/0.3/0.3/0.1$ (full, dashed, pointed, dash-dotted). The top panel shows a region with predominantly weak metal lines, in fact we rely heavily on this region to derive a spectroscopic metallicity. The bottom panel shows a region dominated by strong lines which are clearly insensitive to changes of metallicity in the range discussed here. Note that the synthetic spectra shown here are not folded with instrumental or rotational profiles.

*of the cores of the pseudophotospheric lines are already saturated*. The discrimination becomes more and more difficult with increasing $z_{\rm spec}$. Due to the instrumental profile and stellar projected rotational velocities, these very sharp lines become blurred and the influence of a single line becomes undetectable. Thus one cannot find strategic lines for the determination of the iron group abundances, one has to rely on "strategic blends" for this purpose.

Considering the synthetic spectra convolved with the instrumental profile, shown in Fig. 11, one can see that over large portions of the spectrum a change in the Fe and Ni abundances result in a mere vertical shift. This is most pronounced in the interval from 1305 . . . 1332 Å. Using a "suitable" re-rectification could practically remove the differences between the four spectra there. Thus, from the "overall" better fit for the $z_{\rm spec} = 0.2$ model alone one cannot conclude that this is the best value for

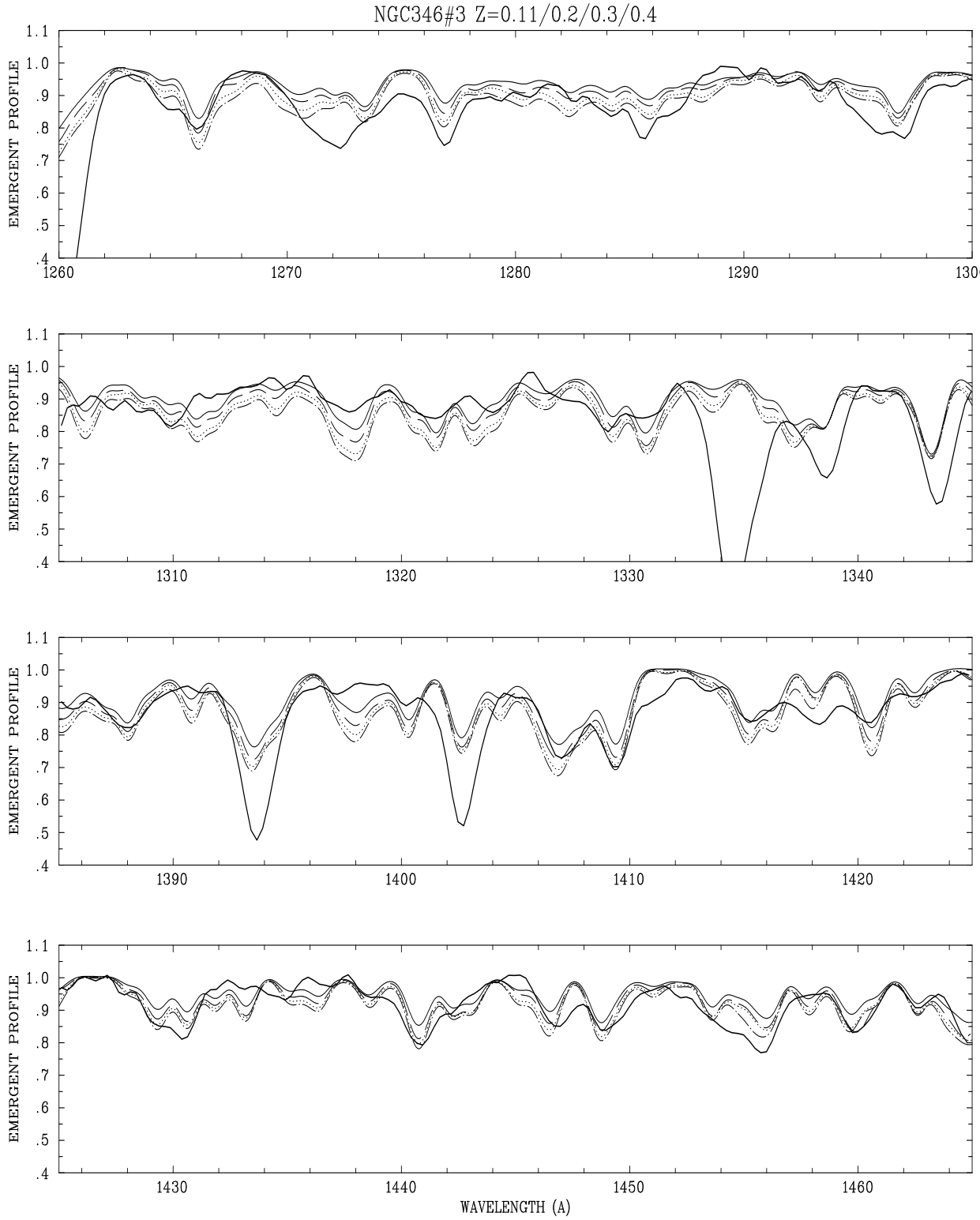


**Fig. 11.** The synthetic spectra for $z_{\rm spec}$ = 0.1/0.2/0.3/0.4, folded with an instrumental profile of FWHM=1 Å, compared with the HST observation, now extended up to 1470 Å (c.f. Fig. 10).

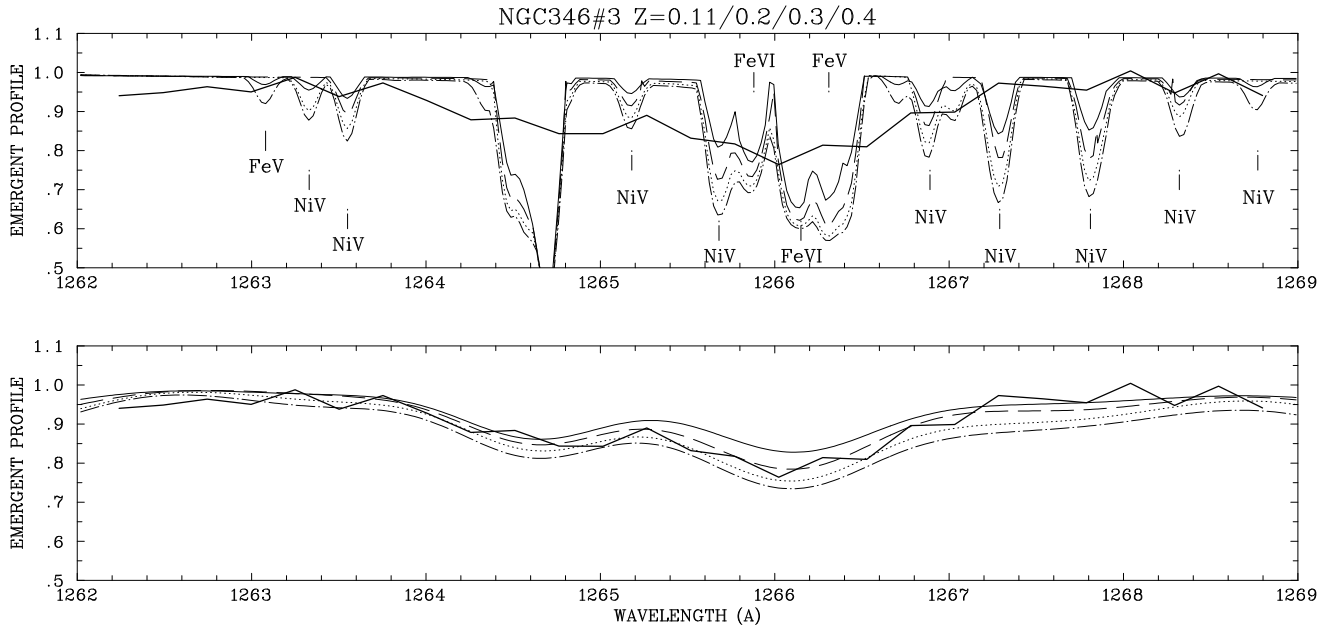


**Fig. 12.** Enlarged portion of Fig. 10 and Fig. 11, now accounting for the interstellar line of Si II$\lambda$1264.74 taken from the IUE spectrum of HD 93129 A. Upper panel: spectrum synthesis not folded; lower panel: spectrum synthesis folded with instrumental profile. Note the unsaturated character of the absorption lines between 1262 und 1270 Å, see text.

**Table 6.** Fe/Ni–lines between 1262 und 1269 Å in the synthetic spectra for NGC 346#3.

| $\lambda$ (Å) | Linie | $\lambda$ (Å) | Linie |
|---|---|---|---|
| 1263.08 | Fe V | 1266.31 | Fe V |
| 1263.33 | Ni V | 1266.40 | Ni V |
| 1263.55 | Ni V | 1266.89 | Ni V |
| 1265.18 | Ni V | 1267.29 | Ni V |
| 1265.68 | Ni V | 1267.81 | Ni V |
| 1265.88 | Fe VI | 1268.32 | Ni V |
| 1266.15 | Fe VI | 1268.77 | Ni V |

the metallicity. In order to be able to derive $z_{\rm spec}$ one must find a feature that fulfils the two following crucial criteria:

*1.* A group of *unsaturated* computed lines must be situated closely together, yet well separated. The region should not contain lines with saturated cores. Thus, the depth of the blend still varies significantly after the convolution to FOS resolution compared to the S/N.

*2.* Such a group of lines must then be in the neighbourhood of a line free or at least line poor region, allowing a good determination of the local continuum. This condition excludes the case of a mere parallel shift of the spectrum.

Only one blend meeting both requirements can be found in the HST spectrum of NGC 346#3. It is shown on a larger scale in Fig. 12. There are 14 intermediately strong lines visible (see Table 6), framed by the nearly line free region at 1262 Å and the line poor region at 1268 Å. Furthermore, none of these lines appears to be saturated in the cores for $z \leq 0.4$.

But yet, this "ideal case" is disturbed by the presence of an interstellar Si II line ($\chi = 287.24\,{\rm cm}^{-1}$) at $\lambda = 1264.74$. Although not recognizable in the FOS spectrum due to the instrumental profile, the following arguments are in favour of the thesis that the weak dip at this very wavelength is indeed of interstellar origin:

A comparison with the IUE spectrum of HD 93129 A shows that the interstellar Si II$\lambda$1527 line in the FOS spectrum of NGC 346#3 is of similar strength when convolved to the same resolution. Also, since the weaker Si II line at 1264.72 Å is clearly visible in the IUE spectrum of HD 93129 A (the resolution of IUE is about a factor of ten higher) it should also show its fingerprint in the FOS spectrum. We have chosen to simulate it by using the same strength as for HD 93129 A. This is undoubtedly a gross overestimate given that HD 93129 A has an extinction of $E(B-V) = 0.54$ compared to 0.09 for NGC 346#3 and this difference probably explains the poor fit in the vicinity of the Si II line. For this reason we do not use this small region of the spectrum to determine $z_{\rm spec}$.

The result is again shown in Fig 12. (Note that this correction has *not* been applied in Figs. 9, 10, and 11). The very strong Si II/S II-blend at 1260 Å also reaches a little into the line free region, its influence, however, is luckily negligible.

It turns out that the local continuum near 1262 Å is indeed identical for all four metallicities, bearing in mind the S/N of $\approx 100$. The same is *not* true for the longward end of the complex $\lambda = 1268$ Å. There the line free regions (in the computed spectra) are all smaller than 1 Å (the instrumental profile width) and thus can never remain unaffected by the convolution, *unless these lines become very weak due to a small metallicity.* In order

to reproduce the flux level there a $z_{\rm spec} > 0.3$ can already be ruled out. The complex at 1266.3 Å now favours $z_{\rm spec}$ = 0.2. Once again we stress that it is exclusively built of unsaturated lines.

Another relatively isolated blend near 1277 Å cannot be used for the determination of $z_{\rm spec}$ since between 1277.24 Å and 1277.9 Å a group of weak interstellar lines of C I is situated ($0 \leq \chi \leq 44\,{\rm cm}^{-1}$). At other wavelengths between 1300 Å and 1470 Å, where more blends of Fe V-VI and Ni V lines are prominent, many features are well or at least qualitatively reproduced, although discrepancies remain. On one hand computed lines of Fe V appear where there are no lines visible in the measurement (1398 Å). On the other hand some blends definitely present are not captured by the calculations (1272, 1285.5, 1411 Å). In some of these cases interstellar contamination might be responsible (see Table 3), or inadequacies in the flat field as discussed above. However, due to the enormous amount of line transitions in the atomic data set, it cannot be ruled out that inaccuracies in wavelengths and/or $gf$-values are responsible. For example, for many lines there are no accurate *measured* wavelengths and one has to rely on the theoretical values. These are sometimes inaccurate by $\Delta\lambda/\lambda \approx 10^{-3}$, resulting in a wavelength shift of about 1 Å or sometimes more. For a number of levels the data have been corrected, but there is still a lot of work to do to improve the atomic data further.

In summary, we conclude that in the case of NGC 346#3, dynamical and spectroscopic metallicities result in a consistent value for the mean metallicity of $z = 0.2 \pm 0.1 z_\odot$. There is strong evidence for the presence of nuclear processed material in the photosphere indicated by an overabundance of nitrogen of a factor of two and underabundance of carbon by a factor of ten relative to the mean metallicity. However, these latter numbers are uncertain by at least a factor of three.

### 5.2. Sk–68° 137

As implied by the nearly identical visual spectral appearance, this star is the LMC counterpart of NGC 346#3. The observed wind momentum rate indicates a metallicity $z_{dyn} \approx 0.6$. For this metallicity (with $\log g_{dyn}$ and the other stellar parameters from Table 1) we have computed a synthetic spectrum, which is shown in Figs. 13. The blocking and $L_{\rm X}$ parameters are given in Table 7.

There is no indication for a deviation from the mean abundances for nitrogen and carbon, contrary to NGC 346#3. The fit for N IV, N V, and C IV can be achieved using appropriate $L_{\rm X}$ and blocking values. However, for O V the same arguments as above apply.

The strength of the features between 1380 and 1500 Å, mainly from Fe V lines, is also reproduced very well, however this is not a strong metallicity constraint, since most of the line cores are saturated. On the other hand, between 1260 and 1300 Å much too strong an absorption appears between the observed blends. As demonstrated by Fig. 14 these are P-Cygni profiles caused by a handful of strong Fe VI lines, which are visible in the wind up to velocities exceeding $0.5\,v_\infty$. The suspicion that this might be due to the large $T_{\rm eff}$ = 60000 K and the therefore high population of Fe VI led us to calculate a cooler model with 55000 K with a metallicity $z_{dyn}$ = 0.4 fitting the observed wind momentum (see Figs 15 and 16). There, the Fe VI lines are still too strong, although substantially weaker. (Note that a similar discrepancy also occurs in the wind analysis of HD 93129 A by Taresch et al. (1997)). The remaining part of the observed spectrum is reproduced equally well by this cooler model.

**Table 7.** Spectrum synthesis parameters for Sk−68° 137.

| $T_{eff}$ | $\log L_{\rm X}$ | $v_{\rm jump}$ | $T_{\rm rad}$/kK | | |
|---|---|---|---|---|---|
| | $[L_{\rm bol}]$ | [km s$^{-1}$] | $< 300$ Å | $< 480$ Å | $< 800$ Å |
| 60000 K | −7 | 190 | 50 | 52 | 36 |
| 55000 K | −7.5 | 190 | 47.5 | 48 | 36 |

**Table 8.** Spectrum synthesis parameters for Sk–67° 166.

| $\log L_{\rm X}$ | $v_{\rm jump}$ | $T_{\rm rad}$/kK | | |
|---|---|---|---|---|
| $[L_{\rm bol}]$ | [km s$^{-1}$] | $< 300$ Å | $< 370$ Å | $< 911$ Å |
| −9.0 | 152 | 41 | 49 | 38 |

The strong Fe VI wind absorption, which is present in the model spectra but is not observed, complicates the use of the 1266 Å complex for a determination of $z_{\rm spec}$, since the local continuum on both sides is not well defined anymore. The low S/N= 20 and the unknown strength of the Si II interstellar absorption do not allow us to separate all these effects. Taking the wind absorption for real, only values for $z_{\rm spec} < 0.3$ could qualitatively reproduce the height of the pseudocontinuum between the blends. On the other hand, the depth of the feature at 1266 Å indicates an abundance $z_{\rm spec}$ = 0.6 or somewhat larger. At the moment we have no definite explanation for this discrepancy, however it is very likely that the Fe VI wind absorption predicted by the models are unrealistic. This would agree with the spectrum synthesis of most of the other blends (see Figs. 13 and 15). We therefore adopt $z_{\rm spec} = 0.5 \pm 0.2 z_\odot$.

### 5.3. Sk–67° 166

The spectroscopic metallicity of $z_{\rm spec} = z_{\rm dyn} = 0.8$ is consistent with the observed iron spectrum of Sk−67° 166 (Fig. 17). The accuracy from the variation in the iron lines is estimated to ±0.3 dex. Note the much weaker Fe VI lines longward of 1260 Å compared to the O3 star Sk−68° 137.

The problem of the O V$\lambda$1371 is still present in this cooler star, although less pronounced. In addition, we now encounter also a problem with the subordinate lines O IV$\lambda\lambda$1339, 1344, N IV$\lambda$1719, which are also too strong. It remains to be examined whether this particular discrepancy can be solved when the selfconsistent treatment of line blocking is applied. The uncertainties in these lines together with the strong saturation of the N V and C IV resonance lines do not allow a more detailed investigation of CNO-abundances.

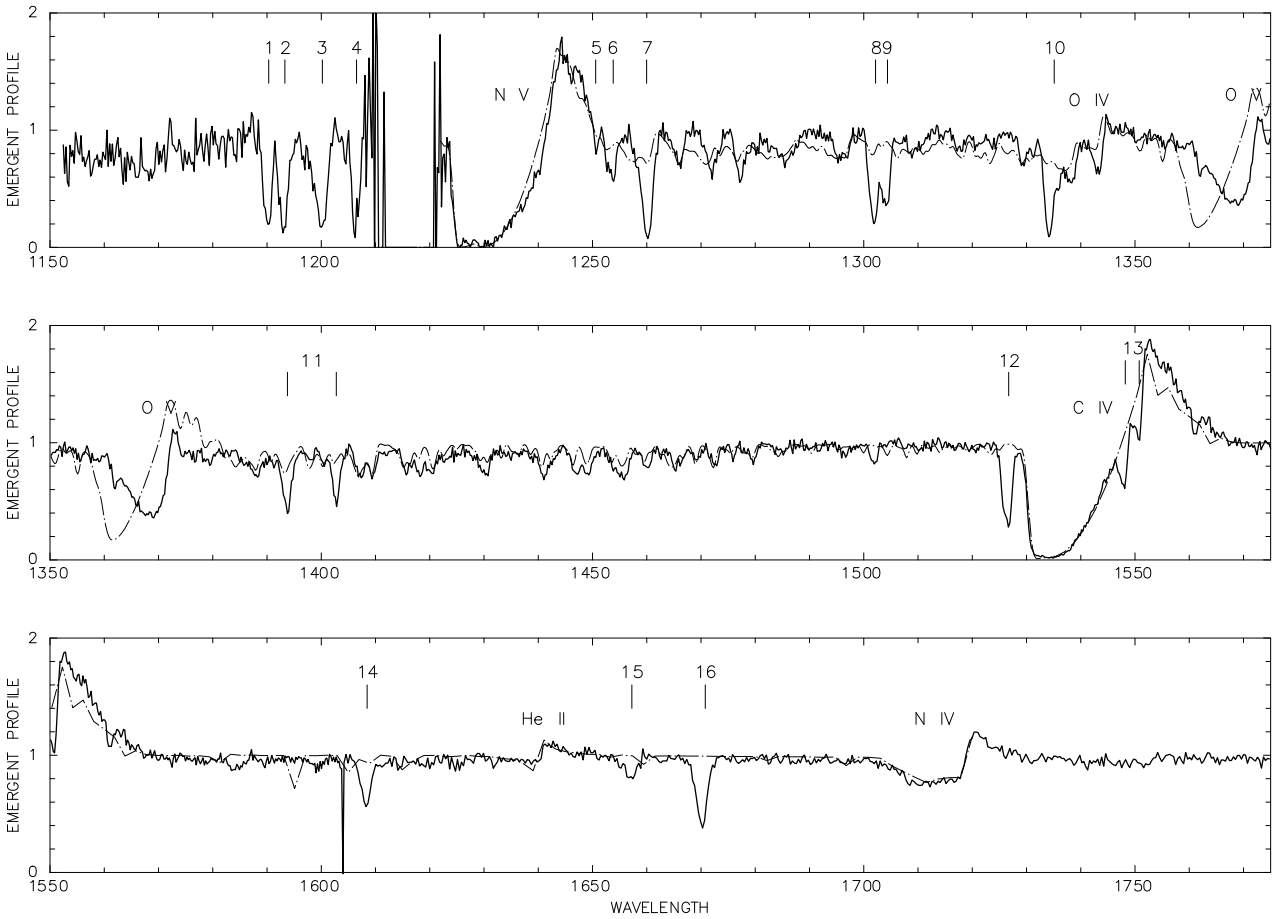


**Fig. 13.** Synthetic spectrum for Sk–68°137 (dash-dotted, $T_{\rm eff}$ = 60000 K, $z$ = 0.6) folded with the instrumental profile and compared with the HST–spectrum). The numbers indicate interstellar absorption lines (see Table 4).

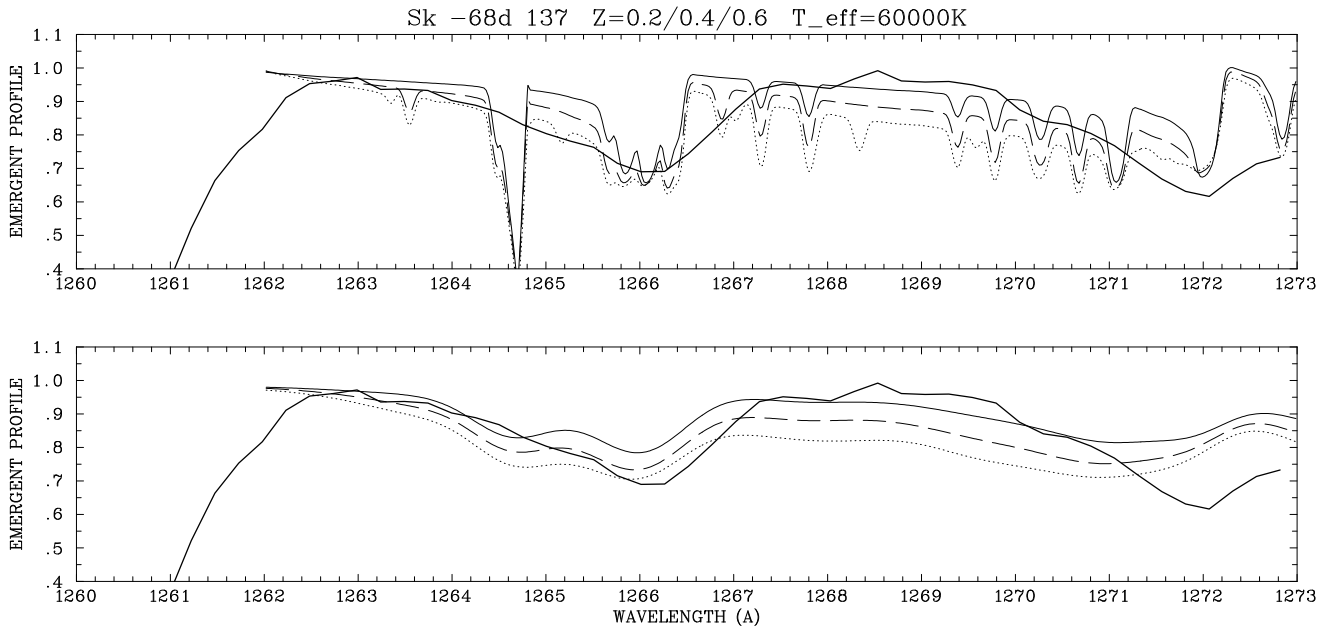


**Fig. 14.** Enlarged portion of Fig. 13 ($z$ = 0.2, 0.4, 0.6, $T_{\rm eff}$ = 60000 K), now also accounting for the interstellar line of Si II$\lambda$1264.74. The difference in the computed spectra is mainly due to the (unsaturated) P-Cygni profiles of Fe VI$\lambda$1266.3 and Fe VI$\lambda$1272. In the lower panel the synthetic spectra are folded with the instrumental profile.

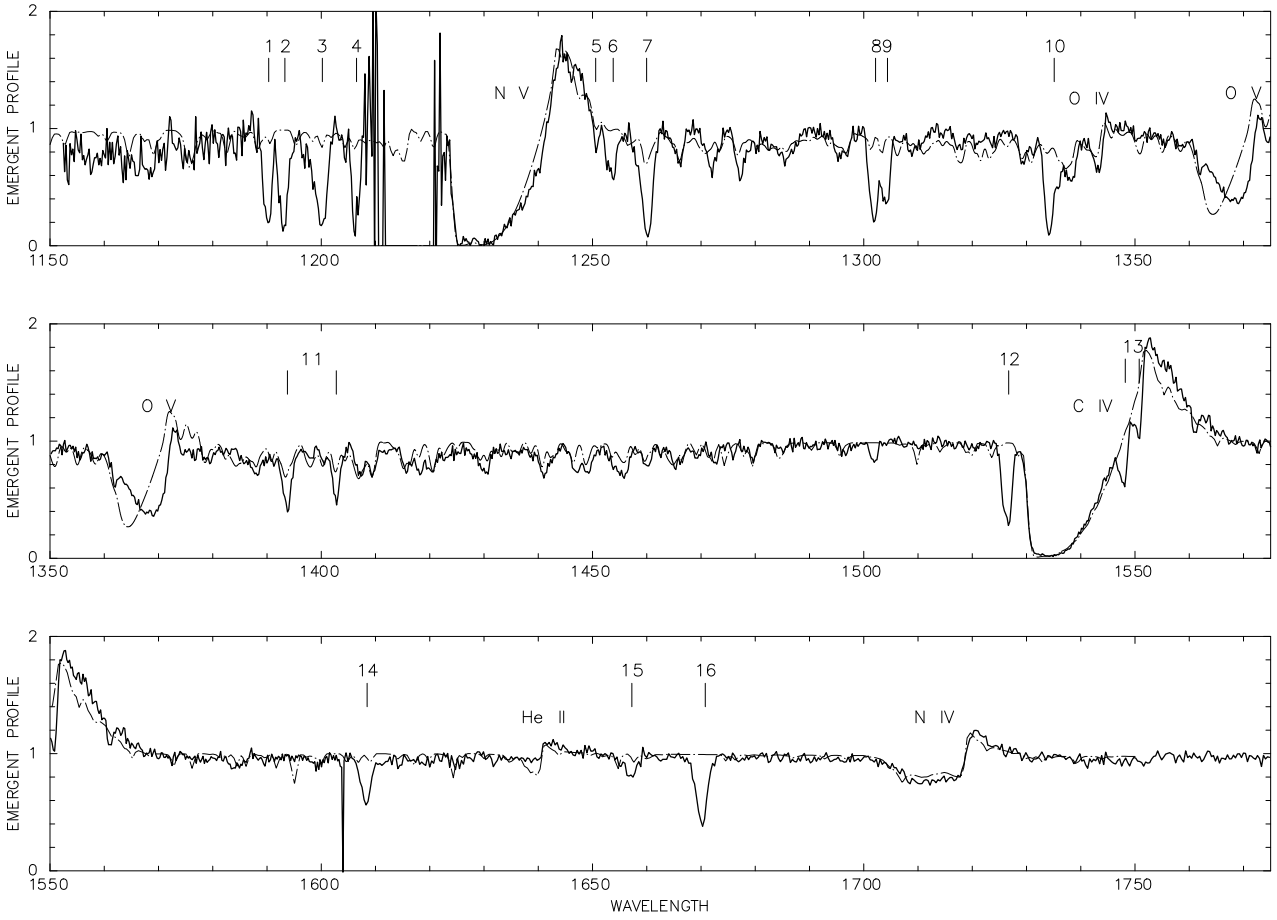


**Fig. 15.** Same as Fig. 13, but calculated spectrum with $T_{\rm eff}$ = 55000 K and $z$ = 0.4.

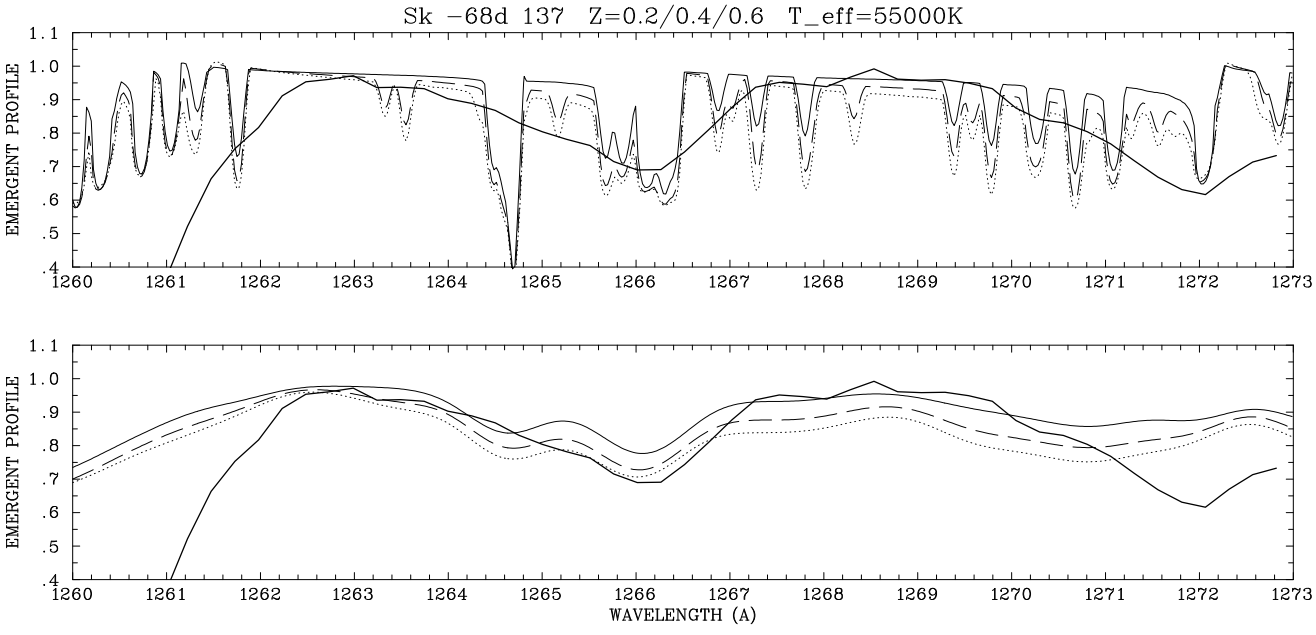


**Fig. 16.** Same as Fig. 14 , but for $T_{\rm eff}$ = 55000 K. Note the weaker wind absorption of Fe VI.

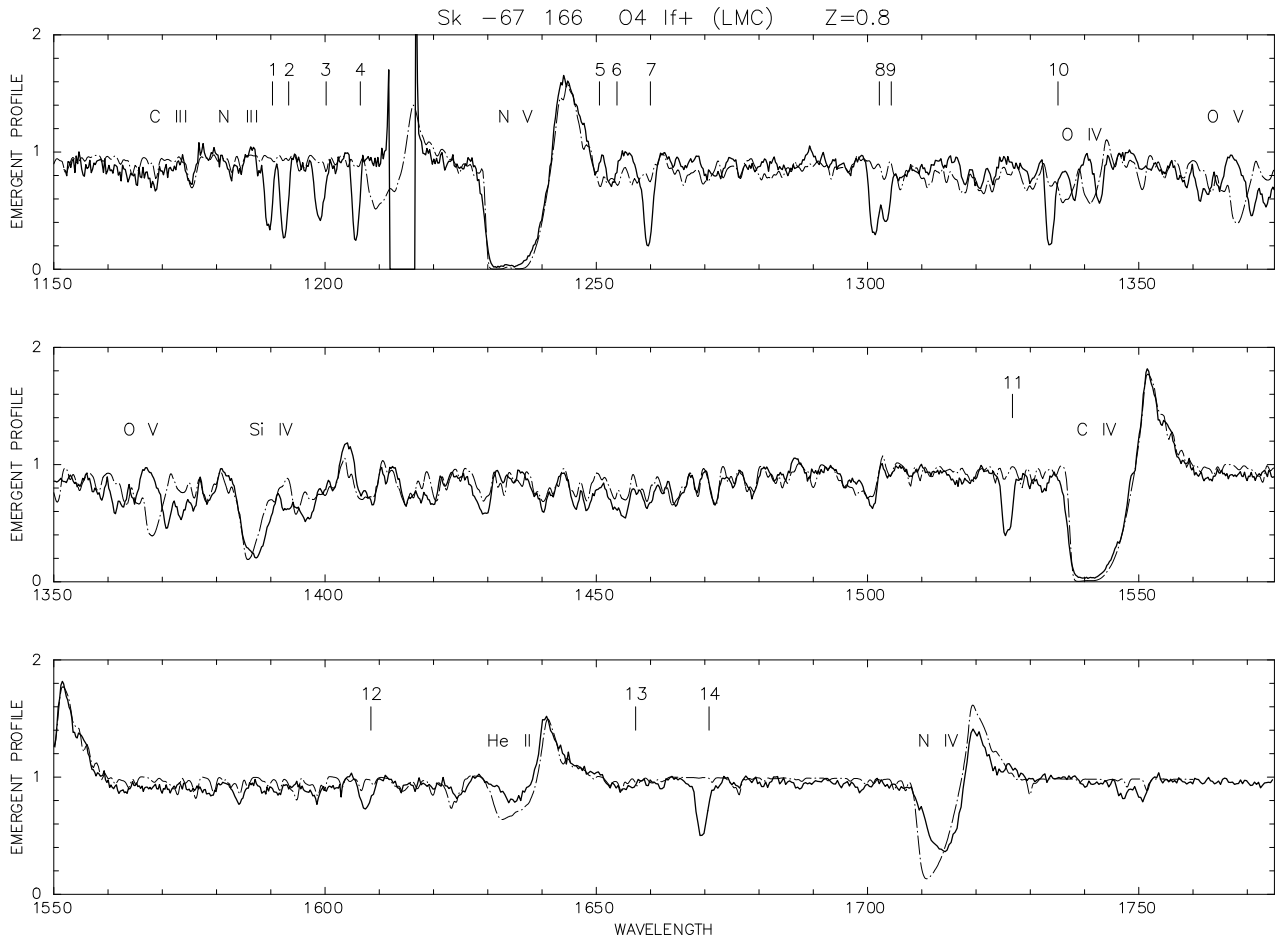


**Fig. 17.** Synthetic spectrum of Sk−67°166 (dash-dotted) folded with the instrumental profile and compared with the HST–spectrum (heavy). The metallicity is $z_{\rm spec}$ = 0.8. The numbers indicate interstellar absorption lines (see Table 4).

### *5.4. AV 243*

We now turn our attention to AV 243 in the SMC, a much cooler object of later spectral type. We have chosen this object out of our sample for two reasons:

*1.* We want to show that the cooler objects offer the possibility for a more precise spectroscopic measurement of their metallicities.

*2.* We want to confirm the above result for NGC 346#3.

We begin with the first of these items. In the spectra of the O3 stars practically no lines of Fe IV are present due to the high $T_{\rm eff}$ and the corresponding high degree of ionization. When going to smaller $T_{\rm eff}$, a shift towards lower ionization occurs. In a certain transition interval of effective temperatures one can thus be certain that *no core saturation occurs in the* Fe IV *lines*, since this ion just starts to get populated. This transition is easily observed in the spectra of galactic O4 – O7 stars where the Fe IV line spectrum shortward of 1510 Å becomes gradually stronger, thus indicating the increase of the ionization fraction of Fe IV (see Haser et al. 1995). The O6 star AV 243 with its relatively moderate but still high $T_{\rm eff}$ = 43500 K may therefore be ideal to demonstrate that the Fe IV line spectrum indeed offers a powerful diagnostical approach for the iron abundance using our spectrum synthesis method.

For the dynamical metallicity, we found $z_{\rm dyn} < 0.1$. However, as already discussed in section 3.1 we expect this value to be unreliable, because, as has been found by Puls et al. (1996), the wind theory predicts too high wind momenta for objects with such low wind performance numbers $\eta$. In consequence, $z_{\rm dyn}$ is very likely too small.

Indeeed, the best spectrum synthesis fit of the overall spectrum is obtained with $z_{\rm spec}$ = 0.2 (see Fig. 18). The comparison with the FOS spectrum in a selected wavelength region and with varying abundances is shown in Fig. 19. (The parameters for the line blocking and the shock emission are given in Table 9). From the latter figure the pronounced metallicity effect on the strength of the Fe IV absorption lines becomes obvious, where the best "by eye" coincidence is given by $z_{\rm spec} \approx 0.1 \ldots 0.2$. Note that to produce this figure we took into account that the continuum normalization of spectra with many dense lines and a broad instrumental or rotational profile is also affected by the metallicity. Thus we have "re-rectified" the synthesized spectra in a few sufficiently wide spectral windows, to best match the computed maxima between the blends. We *then* plotted the dif-

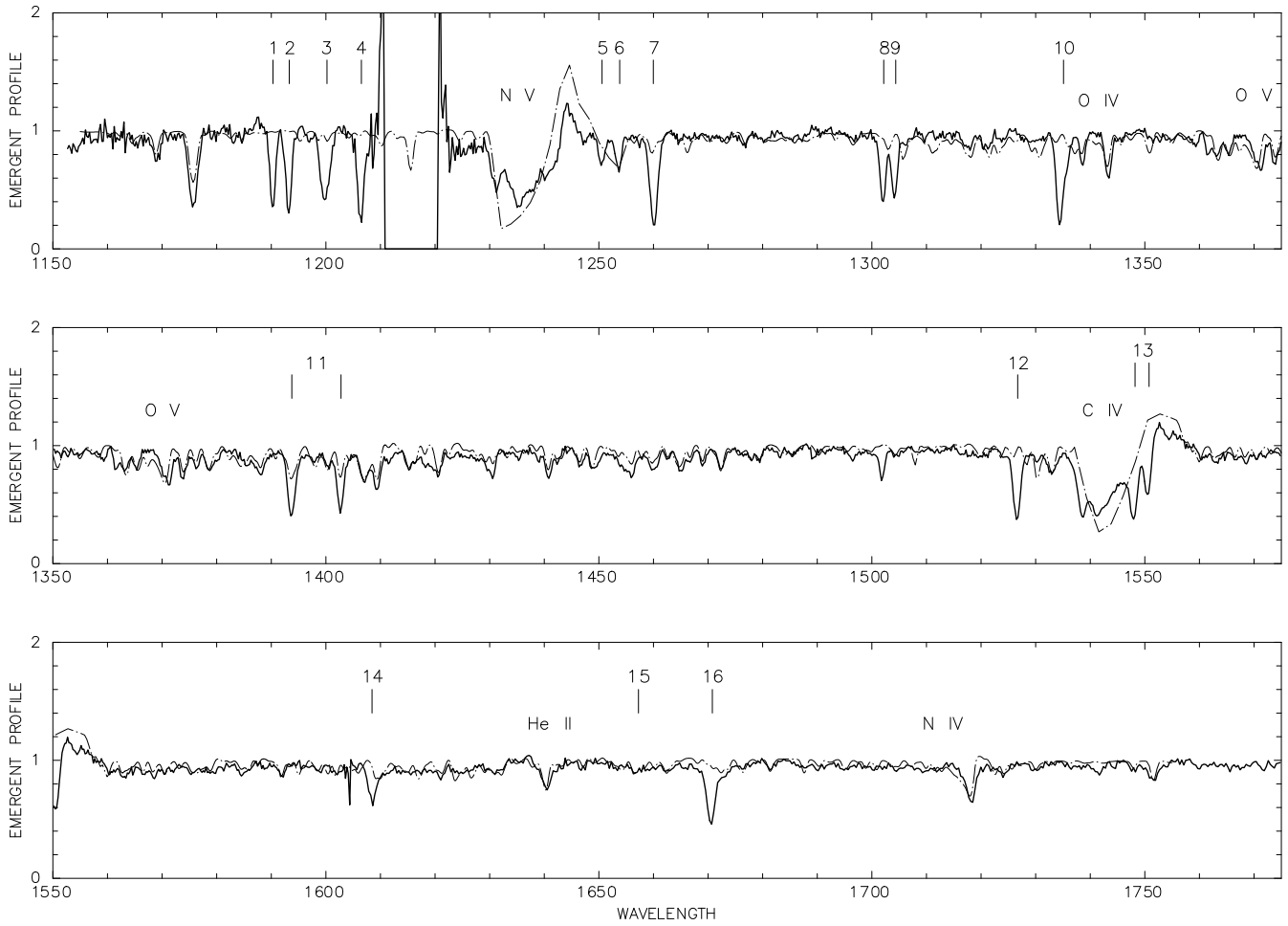


**Fig. 18.** Synthetic spectrum of AV243 folded with the instrumental profile and compared with the HST–spectrum (heavy). The metallicity is $z_{\rm spec}$ = 0.2. The numbers indicate interstellar absorption lines (see Table 4).

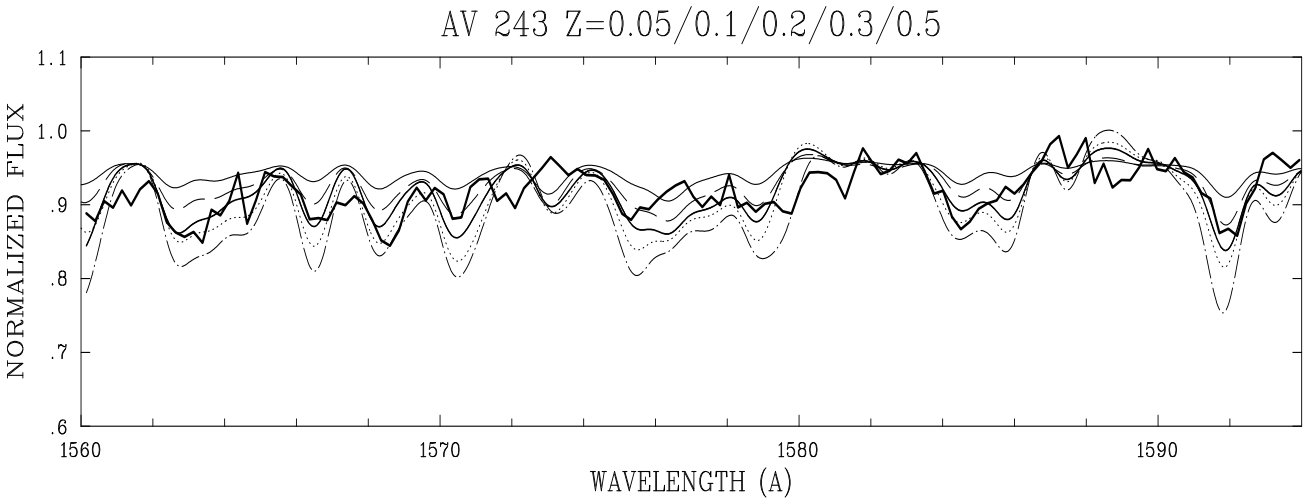


**Fig. 19.** The synthetic spectra for $z_{\rm spec}$ = 0.05 . . . 0.5 (0.05: thin full line, 0.1: dashed, 0.2 medium full line, 0.3: dotted, 0.5: dash-dotted), folded with an instrumental profile of FWHM=1 Åand compared to the HST observation of AV243 (thick line). Note that for this figure the synthetic spectra have been normalized such that after convolution with the instrumental profile the continua at 1565.5 Å, 1582.5 Å, and 1590.0 Å match the continuum of the observed spectrum, see text.

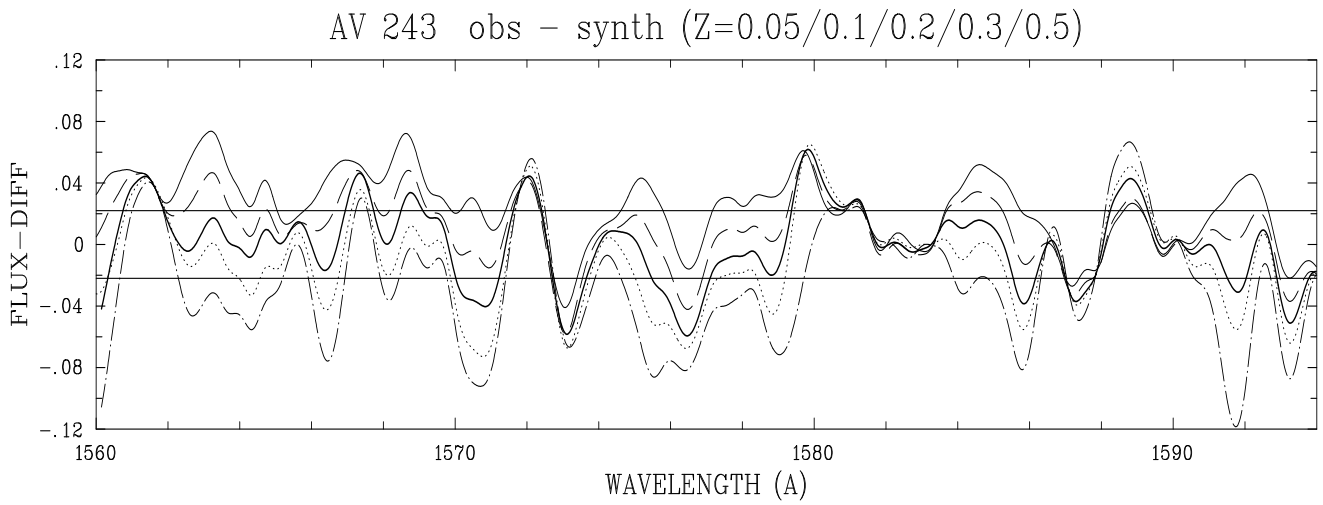


**Fig. 20.** The difference between observed and synthetic spectra for $z_{\rm spec}$ = 0.05 . . . 0.5 in Fig. 19. Again the curve for $z_{\rm spec}$ = 0.2 is highlighted by the thicker line. It shows the least deviation from the zero line. The two horizontal lines indicate the range set by the S/N=45.

**Table 9.** Spectrum synthesis parameters for AV 243.

| $\log L_{\rm X}$ | $v_{\rm jump}$ | $T_{\rm rad}$/ kK | | |
|---|---|---|---|---|
| $[L_{\rm bol}]$ | [km s$^{-1}$] | $< 300$ Å | $< 480$ Å | $< 800$ Å |
| $-7.3$ | 210 | 40 | 41 | 37 |

ference between the observed and the synthetic spectra, shown in Fig. 20. From that kind of representation it is much easier to see, that the spectra with $z_{\rm spec}$ = 0.1 . . . 0.2 are, on the average, closest to the zero line. A check for any correlation between discrepant features and anomalies in the flat field was negative and we therefore conclude that $z_{\rm spec}$ = 0.2 has the smallest average deviation.

We have not shown a similar comparison for the spectral regions shortward of 1500 Å. Although the Fe V lines which dominate there are not saturated, the interplay between the dense line crowding, the instrumental profile and the lower S/N $\approx$ 35 does not allow an improvement of the above result, although the fit looks very convincing for large portions of the spectrum.

The wind lines of CNO are also reproduced rather well in all ionization stages including the problematic lines of O V and O IV . The de-saturated character of C IV and N V would allow a fine tuning of abundances, however it would also be possible to achieve an improvement of the fit by a slight modification of the shock emission (for the parameters see Table 9). The CNO abundances are thus poorly constrained.

In summary, we conclude that the best value for the metallicity is $z_{\rm spec} = 0.15^{+0.15}_{-0.07}$ .

## 6. Discussion and conclusions

We have constructed radiation driven hydrodynamical models for the atmospheres of four O-stars in the Magellanic Clouds to determine their metal abundances, in particular those of the iron group elements. Taking the stellar parameters $T_{\rm eff}$, $\log g$, $R_*$ and the wind parameters $\dot{M}$ and $v_\infty$ from the analysis of the visual spectra and radiative transfer calculations of the UV resonance lines, the metal abundances and surface gravities are treated as free parameters to optimize the wind models such that we reproduce (i) the dynamical quantities $\dot{M}$ and $v_\infty$ and (ii) the morphology of their UV spectra. This process enables us to derive two estimates of the metallicity, which we refer to as their dynamical ($z_{\rm dyn}$) and spectroscopic ($z_{\rm spec}$) values respectively. The latter value corresponds to that which is normally thought of by stellar spectroscopists. The *dynamical* value on the other hand is a new concept taking advantage of the fact that the stellar wind momentum rate is a function of metallicity, as recently discussed by Puls et al. (1996). This new concept still needs verification, since the calculated wind momentum rates may be subject to systematic errors (Lamers & Leitherer 1993, Puls et al. 1996). The results presented here are very encouraging, because we find good agreement for three of our targets, NGC 346#3 (O3 III(f*)) in the SMC and Sk−68°137 (O3 III(f*)) and Sk−67°166 (O4 If+) in the LMC. The dynamical method fails for the SMC dwarf AV 243 (O6 V) with its very weak wind and yields too small a metallicity. This is a consequence of the fact that the theory produces too strong winds for objects of this type, as has already been pointed out by Puls et al. 1996.

We also compare spectroscopic and dynamic gravities, where the former are determined from line profile fits of the optical spectra and the latter follow from dynamical calculations forced to reproduce the terminal velocities $v_\infty$. The dynamical gravities are systematically larger by 0.1 to 0.15 dex. It is not clear at the moment which of the two are more reliable. In view of the determination of stellar masses (see Kudritzki et al., 1992 and Herrero et al., 1992) it will be important to investigate this problem in more detail.

Apart from these discrepancies the results allow one to conclude that our calculations are broadly reproducing the dynam-

ical and spectral properties of O-star winds as a function of metallicity. This conclusion is supported by the fact that with the same approach, Taresch et al. (1997) were also able to reproduce the observed $\dot{M}$ and $v_\infty$ and the pseudophotospheric metal line spectrum of the galactic O3 supergiant HD 93129 A, with a wind model of solar metallicity. This is important for the perspectives discussed further below.

For one object, the SMC O3 III star NGC 346#3 we have found strong evidence for CN processed matter in its atmosphere, with a lower abundance limit of 7.6 dex being found for nitrogen and an upper limit of 6.9 dex for carbon. These values should be compared with Rolleston et al's (1993) determination of abundances for a B-star in the same star cluster resulting in an upper limit for nitrogen of 6.9 dex and a carbon abundance of 7.4$\pm$0.2 dex. The fact that NGC 346#3 has previously been found to have a normal helium abundance (Puls et al 1996), is not necessarily in contradiction to the present results since stellar evolution calculations imply that changes in surface C/N ratios may not always be reflected in significant changes in He/H. Similar results have been found for HD 93129 A in the Galaxy (Taresch et al. (1997)), reinforcing suggestions that mixing processes may occur in O-stars (Langer et al. 1994). Unfortunately, the CNO abundances for the other objects investigated here are not accurate enough to allow any firm conclusions to be reached. This situation stems from the fact that, for all objects, the uncertainties in the CNO abundances are dominated by the inability to constrain the shock properties adequately. In this respect, high resolution observations in the FUV part of the spectrum, including for example the O VI$\lambda\lambda$1032, 1038 lines, would improve matters considerably.

Clearly, for the determination of metal abundances in other resolved galaxies, the use of later type blue supergiants might more easily lead to the desired goal (see McCarthy et al. 1995). However, for the study of unresolved hot stellar populations such as occur in distant starburst galaxies, the construction of synthetic spectra relies upon the use of stellar spectral libraries (Leitherer et al. 1995, 1995). These libraries are based primarily upon solar composition galactic objects, with some attempts to extend this to LMC and SMC metallicities using HST data similar to that discussed here. This is an important point since many starburst galaxies considered so far are metal poor, see for example Vacca & Conti (1992) and Conti et al. (1996). The use of reliable stellar wind models in this kind of population synthesis is obviously extremely important. An additional point is that, although metallicities for starburst galaxies are generally known from H II regions, this refers primarily to their oxygen abundances. We have shown here that it is possible to derive iron abundances from the UV spectra of individual O-stars. An important next step therefore is to test these methods for unresolved populations of O-stars. This will also have important implications for studies of star forming galaxies at high redshift (see for example Steidel et al. 1996) where the ability to compute wind models at arbitrarily low metallicities is a big advantage over the use of stellar spectral libraries limited to metallicities between solar and SMC-like. Given the success of the current investigation, its extension to metallicities outside the range bounded by the Galaxy and the SMC is clearly of high priority.

*Acknowledgements.* We wish to thank our colleagues A. Fullerton, U. Springmann, G. Taresch, and F. Sellmaier for many productive discussions. An incredible lot of motivation has also been provided by Ian, Ian, Jon, Ritchie and Roger. This work was thankfully supported by the Deutsche Forschungsgesellschaft in the "Gerhard Hess Programm" under grant PA 477/1-2 (SMH, ML) and by the Bundesminister für Bildung und Forschung under grant 50 R 93040 (SMH, DJL).

## References

Abbott, D.C. 1979, IAU Symposium 83, S. 237, eds. P.S. Conti, C.W.H de Loore
Becker, S.R., Butler, K. 1992, A&A, 265, 647
Castor, J.I., Abbott, D.C., Klein, R.K. 1975, ApJ, 195, 157
Chlebowski, T., Harnden ,F.R.Jr., Sciortino, S. 1989, ApJ, 341, 427
Conti, P.S., Leitherer, C., Vacca, W. 1996, ApJL, 461, L87
Cox, D.P., Raymond, J.C. 1985, A&A, 298, 615
Feldmeier, A. 1995, A&A, 299, 523
Feldmeier, A., Kudritzki, R.-P., Palsa, R., Pauldrach, A.W.A., Puls, J. 1996, A&A, accepted
Gabler, R. 1991, Ph.D. Thesis, Ludwig-Maximilians-Universität, Munich
Garnett, D.R., Skillman, E.D., Dufour, R.J., Peimbert, M., Torres-Peimbert, S., Terlevich, E., Shields, G.A. 1996, ApJ, 443, 64
Gies, D.R., Lambert, D.L. 1992, ApJ, 387, 673
Haser, S.M., Lennon, D.J., Kudritzki, R.-P., Puls, J., Walborn, N.A., Bianchi, L, Hutchings, J.B. 1994a, Space Sci. Rev., 66, 179
Haser, S.M., Puls, J., Kudritzki, R.-P. 1994b, Space Sci. Rev., 66, 187
Haser, S.M., Lennon, D.J, Kudritzki, R.-P., Puls, J., Pauldrach, A.W.A., Bianchi, L., Hutchings, J.B. 1995, A&A, 295, 136
Haser, S.M. 1995, Ph.D. Thesis, Ludwig-Maximilians-Universität, Munich
Herrero, A., Kudritzki, R.-P., Vilchez, J.M., Kunze, D., Butler, K., Haser, S.M. 1992, A&A, 261, 209
Hunsinger, J. 1993, Diploma Thesis, Ludwig-Maximilians-Universität, Munich
Jannuzi, B.T., Hartig, G.F. 1993, in Calibrating Hubble Space Telescope, ed. J.C. Blades & S.J. Osmer, STScI, p215
Keyes, C.D. 1993, in Calibrating Hubble Space Telescope, ed. J.C. Blades & S.J. Osmer, STScI, p209
Kilian, J. 1992, A&A, 262, 171
Kilian, J. 1994, A&A, 282, 867
Kronberg, A. 1996, Diploma Thesis, Ludwig-Maximilians-Universität, Munich
Kudritzki, R.-P., Pauldrach, A., Puls,J. 1987, A&A, 173, 293
Kudritzki, R.-P., Hummer, D.G., Pauldrach, A.W.A., Puls, J., Najarro, J., Imhoff, J. 1992, A&A, 257, 655
Kudritzki, R.-P., Lennon, D.J., Puls,J. 1995, in: *"Science with the VLT"* eds. J.R. Walsh, I.J. Danziger, Springer-Verlag, p. 246
Kudritzki, R.P., Lennon, D.J., Haser, S.M., Puls, J., Pauldrach, A., Venn, K., & Voels, S.A. 1996a, in: *"Science with the Hubble Space Telescope II"* eds. P. Benvenuti et al., 285–296
Kudritzki, R.P. 1996, in: *"Wolf-Rayet Stars in the Framework of Stellar Evolution"* eds. J.M. Vreux et al., 467–489
Kurucz, R.L. 1992, Rev. Mex. Astron. Astrof., 23, 181
Lamers, H.J.G.L.M., Leitherer, C. 1993, ApJ, 412, 771
Langer, N., Hamann, W.-R., Lennon, M., Najarro, F., Pauldrach, A.W.A, Puls, J. 1994, A&A, 290, 819

Langer, N., Maeder, A. 1995, A&A, 295, 685
Leitherer, C., Robert, C., Drissen, L. 1992, ApJ, 401, 596
Leitherer, C., Robert, C., Heckman, T.M. 1995, ApJS, 99, 73
Lindler, D., Bohlin, R., Hartig, G., Keyes, C. 1993, FOS Instrument Science Report CAL/FOS-088
Lucy, L.B., Solomon, P.M. 1970, ApJ, 159, 879
Lucy, L.B. 1982, ApJ, 255, 278
Maeder, A. 1991, A&A¡ 242, 93
Maeder, A., 1991b,in: *"Massive stars in starbursts"*, eds. C. Leitherer, N.R. Walborn, T.M. Heckman, and C.A. Norman, STScI Symposium Series, 5., Cambridge University Press, Cambridge, p. 97
Maeder, A., 1996,in: *"From stars to galaxies: The impact of stellar physics on galaxy evolution"*, eds. C. Leitherer, U. Fritze-von Alvensleben, J. Huchra, ASP Conf. Ser., Vol. 98, p. 141
Maeder, A., Conti, P., 1994, Ann. Rev. A&A, 32, 277
McCarthy, J.K, Lennon, D.J., Venn, K.A., Kudritzki, R.-P., Puls, J., Najaro, F. 1996, ApJL, 455, L35
Morton, D.C. 1991, ApJS, 77, 119
Owocki, S.P., Castor, J.I., Rybicki, G.B. 1988, ApJ, 368, 261
Owocki, S.P. 1992, *Instabilities in Hot-Star Winds: Basic Physics and Recent Developments*, in: Atmospheres of Early-Type Stars, eds.: U. Heber, S. Jeffery, Springer-Verlag, Heidelberg,
Palsa, R., Kudritzki, R.P., Feldmeier, A., Puls, J., Pauldrach, A.W.A. 1996, in prep. for A&A
Pauldrach, A.W.A., Puls, J., Kudritzki, R.-P. 1986, A&A, 164, 86
Pauldrach, A.W.A. 1987, A&A, 183, 295
Pauldrach, A.W.A., Puls, J. 1990, A&A, 237, 409
Pauldrach, A.W.A., Kudritzki, R.-P., Puls, J., Butler, K. 1990, A&A, 228, 125
Pauldrach, A.W.A., Feldmeier, A., Puls, J., Kudritzki, R.-P. 1994a, Sp. Sci. Rev., 66, 105
Pauldrach, A.W.A., Kudritzki, R.-P., Puls, J., Butler, K., Hunsinger, J. 1994b, A&A, 283, 525
Pauldrach, A.W.A., Duschinger, M., Mazzali, P.A., Puls, J., Lennon, M., Miller, D.L. 1996, A&A, 312, 525
Puls, J. 1987, A&A, 184, 227
Puls, J., Pauldrach, A.W.A. 1990, *(New) Methods of Radiative Transfer in Expanding Atmospheres*, in: Astronomical Society of the Pacific Conference Series, Vol. 7, ("Boulder Munich Workshop"), ed. C. Garmany, San Francisco, S. 203
Puls, J., Owocki, S.,P., Fullerton, A.W. 1993, A&A, 279, 457
Puls,
J. , Kudritzki, R.-P., Herrero, A., Pauldrach, A.W.A., Haser, S.M., Lennon, D.J., Gabler, R., Voels, S.A., Wachter, S., Feldmeier, A. 1996, A&A, 305, 171
Raymond, J.C., Smith, B.W. 1977, ApJS, 35, 419
Russell, S.C., Bessell, M.S. 1989, ApJS, 70, 865
Savage, B.D., Sembach, K.R. 1996, ARAA, 34, 279
Schaller, G., Schaerer, D., Meyent, G., Maeder, A. 1992 A&AS, 96, 269
Sellmaier, F.H. 1996, Ph.D. Thesis, Ludwig-Maximilians-Universität, Munich
Sellmaier, F.H., Yamammoto, T., Pauldrach, A.W.A., Rubin, R.H. 1998, A&A Lett., 305, L37
Seward, F.D., Forman, W.R., Giacconi, R., Griffiths, R.E., Harnden, F.R., Jones, C., Pye, J.P. 1979, ApJL, 234, L55
Simpson, J.P., Colgan, S.W.J., Rubin, R.H., Erickson, E.F., Hass, M.R. 1995, ApJ, 444, 721
Steidel, C.C., Giavalisco, M., Pettini, M., Dickinson, M., Adelberger, K.L. 1996, ApJL, 462, L17
Taresch, G., Kudritzki, R.-P., Hurwitz, M., Bowyer, S., Pauldrach, A.W.A., Puls, J., Butler, K., Lennon, D.J., Haser, S.M. 1997, A&A, in press
Vacca, W. Conti, P.S. 1992, ApJ, 401, 543
Venn, K.A. 1996, ApJ, submitted
Walborn, N.R., Lennon, D.J., Haser, S.M., Kudritzki, R.-P., Voels, S.A. 1995a, PASP, 707, 104
Walborn, N.R., Long, K.S., Lennon, D.J., Kudritzki, R.-P. 1995b, ApJL, 454, L30

This article was processed by the author using Springer-Verlag LaTeX A&A style file *L-AA* version 3.